Title: HBV Remodels PP2A Complexes to Rewire Kinase Signaling in Hepatocellular Carcinoma

Authors: Rigney E Turnham[1,2]*, Adriana Pitea[3]*, Gwendolyn M Jang[2,4], Zhong Xu[5], Huat Chye Lim[1,2], Alex L Choi[1,2], John Von Dollen[2,4], Rebecca S. Levin[4], James T Webber[5], Elizabeth McCarthy[4], Junjie Hu[5], Xiaolei Li[5], Li Che[5], Ananya Singh[1,2], Alex Yoon[1,2], Gary Chan[1,2], Robin K Kelley[1], Danielle L Swaney[2,4], Wei Zhang[3], Sourav Bandyopadhyay[5], Fabian J Theis[6], Manon Eckhardt[2,4,7], Xin Chen[5], Kevan M Shokat[2,4,8], Trey Ideker[3]†, Nevan J Krogan[2,4,9,10]†, John D Gordan[1,2]†

*Equal contribution

Affiliations:
[1]Division of Hematology/Oncology, University of California, San Francisco CA
[2]Quantitative Biosciences Institute, University of California, San Francisco CA
[3]Department of Medicine, University of California, San Diego, La Jolla, CA
[4]Department of Cellular and Molecular Pharmacology, University of California, San Francisco CA
[5]Department of Bioengineering, University of California, San Francisco CA
[6]TUM School of Life Sciences, Technical University of Munich, Munich, Germany.
[7]Gladstone Institute of Data Science and Biotechnology, J. David Gladstone Institutes, San Francisco, CA
[8]Howard Hughes Medical Institute, University of California, San Francisco CA
[9]Department of Bioengineering and Therapeutic Sciences, University of California, San Francisco
[10]Gladstone Institute of Data Science and Biotechnology, J. David Gladstone Institutes, San Francisco, CA

†To whom correspondence should be addressed: TI: tideker@health.ucsd.edu; NJK: nevan.krogan@ucsf.edu; JDG: john.gordan@ucsf.edu

Primary Corresponding author's contact information:
John Gordan, MD PhD
University of California, San Francisco
1700 4th Street
San Francisco, CA 94143
P: (415) 476-3252

Keywords: Hepatitis B Virus; Host-virus interactions; systems biology; protein phosphatase 2A; liver cancer

Conflict of Interest: No relevant conflicts of interest.

Financial Support: JDG was supported by an American Cancer Society Postdoctoral Fellowship, Conquer Cancer Foundation Young Investigator Award and Burroughs Wellcome Fund Career Award. KMS is supported by the NIH (RO1 A130699), and HHMI. RT was supported by the Hope Funds for Cancer Research (HCFR-21-05-05) and National Center for Advancing Translational Sciences (TR001871). AP was funded by the Joachim Herz Foundation with the Add-On Fellowship for Interdisciplinary Life Science. XC is supported by NIH grants R01CA136606 and R01CA190606. NJK and RKK were supported by the UCSF Program for Breakthrough Biomedical Research.

Author contributions: Concept and design: JDG, ME, TI, NJK, KMS, XC, WZ, SB, RKK, Experiments and procedures: JDG, AP, RET, ME GMJ, ZX, ALC, JVD, RSL, JTW, HCL, EM, JH, XL, LC, AS, ASY, GC, JC, DS, FJT, WZ; Writing of article: JDG, ME, RET, AP

Words of main text (excluding Methods): 4638
Figures: 6

Downloaded from http://aacrjournals.org/cancerres/article-pdf/doi/10.1158/0008-5472.CAN-24-0456/3524752/can-24-0456.pdf by CDL - University of California - San Diego user on 10 January 2025

53 **Abstract**
54 Hepatitis B virus (HBV) infections promote liver cancer initiation by inducing inflammation and cellular stress.
55 Despite the primarily indirect effect on oncogenesis, HBV is associated with a recurrent genomic phenotype in
56 HCC, suggesting that it impacts the biology of established HCC. Characterization of the interaction of HBV with
57 host proteins and the mechanistic contributions of HBV to HCC initiation and maintenance could provide insights
58 into HCC biology and uncover therapeutic vulnerabilities. Here, we used affinity purification mass spectrometry
59 to comprehensively map a network of 145 physical interactions between HBV and human proteins in
60 hepatocellular carcinoma (HCC). A subset of the host factors targeted by HBV proteins were preferentially
61 mutated in non-HBV-associated HCC, suggesting that their interaction with HBV influences HCC biology. HBV
62 interacted with proteins involved in mRNA splicing, mitogenic signaling, and DNA repair, with the latter set
63 interacting with the HBV oncoprotein X (HBx). HBx remodeled the PP2A phosphatase complex by excluding
64 striatin regulatory subunits from the PP2A holoenzyme, and the HBx effects on PP2A caused Hippo kinase
65 activation. In parallel, HBx activated mTOR complex 2 (mTORC2), which can prevent YAP degradation.
66 mTORC2-mediated upregulation of YAP was observed in human HCC specimens and mouse HCC models and
67 could be targeted with mTOR kinase inhibitors. Thus, HBV interaction with host proteins rewires HCC signaling
68 rather than directly activating mitogenic pathways, provide an alternative paradigm for the cellular effects of a
69 tumor promoting virus.
70

71 **Significance**
72 Integrative proteomic and genomic analysis of HBV/host interactions illuminated modifiers of hepatocellular
73 carcinoma behavior and key signaling mechanisms in advanced disease, which suggested that HBV may have
74 therapeutically actionable effects.

Downloaded from http://aacrjournals.org/cancerres/article-pdf/doi/10.1158/0008-5472.CAN-24-0456/3524752/can-24-0456.pdf by CDL - University of California - San Diego user on 10 January 2025

75 **Introduction**
76 Hepatocellular carcinoma (HCC) is a leading cause of cancer death worldwide (1). Comprehensive genomic
77 profiling of HCC has revealed only a low incidence of targetable driver mutations (2,3). Accordingly, HCC
78 treatment is currently directed at common disease features such as angiogenesis or immune evasion (4).
79 Although FGF19 amplification has been validated as a targetable driver in HCC (5), there are currently no
80 molecularly targeted agents in use for HCC and further investigation is required to identify targetable
81 mechanisms of HCC growth.
82
83 The majority of HCC arises in the setting of co-morbid hepatitis due to viral infection caused by hepatitis B or
84 hepatitis C viruses (HBV or HCV), or metabolic disorders such as non-alcoholic steatohepatitis (2,3). Some
85 tumor-associated viruses exert direct effects on tumor maintenance, such as the degradation of *TP53* by Human
86 Papilloma Virus (HPV) E6 (6). Hepatitis viruses primarily promote tumor initiation via increased local
87 inflammation and cell turnover (2,3,7). The timeline for HBV- and HCV-induced tumorigenesis in murine models
88 is consistent with an indirect role, with viral proteins causing HCC with >1 year latency (8). In contrast, HPV
89 protein expression causes papillomatosis in mice within 2-3 months (9). Despite its primarily indirect effect on
90 oncogenesis, we and others have identified a recurrent HBV-associated genomic phenotype in HCC (2,3,10)
91 suggesting that it significantly impacts the biology of established HCC.
92
93 HBV is a small, enveloped DNA virus which expresses a surface antigen (HBs), core protein (HBc), polymerase
94 (Pol) and a putative oncogenic effector protein, HBV protein X (HBx). Pol is the only HBV protein with enzymatic
95 activity, functioning to initiate minus strand DNA synthesis and reverse transcribe viral RNA intermediates back
96 into DNA. HBc forms the viral capsid around the HBV genome, with surface antigen mediating hepatocyte binding
97 (7,11). HBx has been ascribed many functions that may promote oncogenesis, including activating the kinase
98 AKT (7). HBx is also necessary for HBV replication based on its ability to hijack the CRL4 E3 ubiquitin ligase
99 (12,13). This effect of HBx has been connected to disrupted DNA-damage repair (14). Earlier, members of this
100 team reported a complete HCV protein-protein interaction (PPI) map (15). In contrast to what is known about
101 HBx, there is no suspected HCV oncogenic effector, and few PPIs are seen with cancer-relevant proteins.
102
103 The distinct phenotype of HBV-associated HCC and putative oncogenic effects of HBV proteins motivate further
104 study to characterize HBV's interaction with host proteins and thus its mechanistic contributions to HCC initiation
105 and maintenance. Integrative models of multilevel data are well-suited to study the complex interactions between
106 cancer and infectious diseases. We have previously used a similar approach where we integrated host/HPV
107 PPIs with cervical and oropharyngeal cancer genomics This strategy enabled identification of cancer pathways
108 that are modulated either by HPV in virus-associated tumors or by somatic mutations in non-viral tumors (6).
109 Here, we extend this strategy to HBV and its impact on HCC, further advancing the analytical workflow to address
110 the marked mutational heterogeneity of HCC. This approach yields new insights into HCC biology and
111 demonstrates potent effects of HBV on HCC tumor cell biology, supporting the possibility that HBV infection may
112 result in therapeutic vulnerabilities.
113
114 **Materials and Methods**
115
116 Cell culture and treatments
117 Hep3B (RRID:CVCL_0326), HepG2 (RRID:CVCL_1098), SNU-182 (RRID:CVCL_0090), SNU-387
118 (RRID:CVCL_0250), SNU-398 (RRID:CVCL_0077), SNU-423 (RRID:CVCL_0366), SNU-449
119 (RRID:CVCL_0454), SNU-475 (RRID:CVCL_0497), and PLC/PRF/5 (RRID:CVCL_0485) were obtained from
120 ATCC (Manassus, VA). HUH7 (RRID:CVCL_0336) was obtained from the UCSF Cell Culture Facility and HUH6
121 was obtained from the RIKEN cell bank (Tsukuba, Japan). HLE (RRID:CVCL_1281), HLF (RRID:CVCL_2947),
122 FOCUS (RRID:CVCL_7955) and Hep40 (RRID:CVCL_EI25) were obtained from Dr. Ju-Seog Lee (MD Anderson
123 Cancer Center). MHCC97-H (RRID:CVCL_4972) and MHCC97-L (RRID:CVCL_4973)were obtained from
124 Zhongshan Hospital of Fudan University, Shanghai. Cells were cultured in DMEM with high glucose (Invitrogen,
125 Carlsbad CA) with 10% fetal calf serum (Axenia BioLogIx, Dixon CA) for all experiments, with SNU-182, SNU-
126 387, SNU-398, SNU-423, SNU-449, SNU-475 passaged in RPMI/10% FCS. Puromycin selections were
127 performed at 1 μG/mL and hygromycin selections at 50 μG/mL. Cells were stably maintained in selection
128 conditions. Everolimus, LB-100, MG-132, MK-2206, okadaic acid and TAK-228 and were obtained from

Downloaded from http://aacrjournals.org/cancerres/article-pdf/doi/10.1158/0008-5472.CAN-24-0456/3524752/can-24-0456.pdf by CDL - University of California - San Diego user on 10 January 2025

129 Selleckchem (Houston, TX), and E-1035 synthesized following established protocols (16). Cells were maintained
130 for 10 or fewer passages and monitored no less than quarterly for mycoplasma contamination and identity
131 confirmed with STR on receipt if not purchased from ATCC. STR was repeated if changes in morphology or
132 behavior were noted or before key experiments such as screens. Key cell lines were also confirmed by STR at
133 final submission.
134

135 Mouse models

136 Wild-type (WT) FVB/N mice were obtained from Charles River Laboratories (Wilmington, MA) and *Rictor*$^{fl/fl}$ mice
137 from The Jackson Laboratory (Sacramento, CA). Hydrodynamic injection was performed as previously (17). We
138 injected 60μg pT3-EF1α-Cre or 60μg pT3-EF1α (empty vector control) together with 20μg pT3-EF1α-HA-myr-
139 AKT and 20μg pT2-Caggs-RasV12 to delete *Rictor* while co-expressing AKT and Ras. Mice were housed, fed,
140 and monitored in accord with protocols approved by Institutional Animal Care and Use Committee at the
141 University of California, San Francisco (San Francisco, CA), and were monitored for signs of morbidity.
142

143 Gene mutation analysis

144 To determine which protein coding genes were altered in the LIHC TCGA data set, we used the corresponding
145 mutation data files and copy number calls on gene level provided by the Broad Institute TCGA GDAC. The
146 mutation annotation file comprised 53,777 missense mutations as determined by Mutation Assessor (18) in
147 14,901 RNAs and 373 patients. We classified genes as altered (Mut) or wild type (WT) as follows: We removed
148 variants classified as ['Silent', 'IGR', '5'UTR', '3'UTR', '5'Flank', '3'Flank', 'RNA', 'Intron'], yielding 41,263 non-silent
149 mutations across 13,675 genes. Additionally, we considered genes with amplifications or deletions as
150 determined by GISTIC as mutated. Once mutations/CNAs were identified, we intersected them with the protein
151 coding genes included in the ReactomeFI PPI reference network (https://reactome.org/). As a result, we
152 determined m=8,765 protein coding genes altered by either mutations, amplifications or deletions, in a set of
153 n=366 patients. Patients with HBV and HCV co-infection were excluded. For the following analysis, we binarized
154 this information for each gene: [0=WT, 1=Mut].
155

156 Differential mutation analysis

157 To determine the effect of the viral infections on the mutational status of each gene in HCC, we assessed the
158 differential mutation rates at gene level between:
159

160 A. HCV(+) and HCV(-) HCC cases.
161 B. HBV(+) and HBV(-) HCC cases.
162

163 For this purpose, we set up to map the inputs $x_{g_{hepB}}$, $x_{g_{hepC}}$ to the output y_g, where $g \epsilon \{g_1, \dots, g_m\}$. The output y_g
164 is a one dimensional ($1d$) vector of length n representing the mutational status across the n HCC patients for
165 each mutated gene g (0 = wild type; 1 = altered). The features $x_{g_{hepB}}$ and $x_{g_{hepC}}$ are $1d$ binary vectors of length
166 n representing the viral infection status for HCV (1 = HCV(+); 0 = HCV(-)) -- $x_{g_{hepC}}$, and the viral infection status
167 for HBV (1 = HBV(+); 0 = HBV(-)) -- $x_{g_{hepB}}$.
168

169 Given the response variable y_g is binary, and we aimed to learn the impact of the viral infections on the mutation
170 status, the first choice to formalize the problem was logistic regression. However, logistic regression returned
171 perfect separation of the response which is a common problem in small sample size studies and imbalanced
172 data. Perfect separation is accompanied by unstable regression coefficients, and can yield misleading findings.
173 Since our aim was to estimate the risk of a mutation happening due to viral infection, and not to solve a binary
174 classification problem, we used the solution proposed by Gelman et al. to obtain stable regression coefficients
175 (19). Following, we formally defined three Bayesian logistic regression models conditioned by independent
176 Student-t prior distributions on the coefficients for each g out of the m mutated protein coding genes:

Downloaded from http://aacrjournals.org/cancerres/article-pdf/doi/10.1158/0008-5472.CAN-24-0456/3524752/can-24-0456.pdf by CDL - University of California - San Diego user on 10 January 2025

177
178 $$\pi_{g_{complete}}: p\left(y_g | x_{g_{hepB}}, x_{g_{hepC}}\right)$$
179 $$\pi_{g_{null_1}}: p\left(y_g | x_{g_{hepC}}\right)$$
180 $$\pi_{g_{null_2}}: p\left(y_g | x_{g_{hepB}}\right),$$
181
182
183 where $\pi_{g_{complete}}$is defined by the probability mass function of the output $y_g$given $x_{g_{hepC}}$and $x_{g_{hepB}}$, $\pi_{g_{null_1}}$is defined
184 by the probability mass function of the output y_g given $x_{g_{hepC}}$, and $\pi_{g_{null_2}}$ is defined by the probability mass
185 function of the output y_g given $x_{g_{hepB}}$ only. We used the default Cauchy distribution with mean 0 and prior scale
186 2.5 -- in the simplest scenario, a longer-tailed version of the distribution attained by assuming one-half additional
187 success and one-half additional failure in a logistic regression.
188 To examine the impact of HBV infection on mutational status of HCC tumors, we compared the likelihood of the
189 $\pi_{g_{complete}}$model to the likelihood of each of the two alternative models. Hence, we calculated the deviances
190 between the complete model and each of the two alternative models:
191
192 $$D_{g_{hepB}} = -2ln\left(\frac{L_{g_{null1}}}{L_{g_{complete}}}\right)$$
193 $$D_{g_{hepC}} = -2ln\left(\frac{L_{g_{null2}}}{L_{g_{complete}}}\right)$$
194
195 with *L* being the maximum likelihood, i.e. the probability of the data given the inputs x_g and the parameter vector
196 θ that maximizes $p\left(y_g|\theta, x_g\right) = \prod_{i=1}^{n} \quad p\left(y_{g_i}|\theta, x_{g_i}\right)$,with n representing the number of samples. Our code is
197 available on Github (https://github.com/adspit/HBV_HCC_interaction_inference).
198
199 ## Affinity Purification – Mass Spectrometry:
200 Affinity purification was performed as previously described (6,20). Briefly, HUH7 cells were transfected with
201 FuGene 6 (Promega, Madison WI), and cell pellets were harvested 40 hours after transfection. Clarified cell
202 lysates were incubated with prewashed Strep-Tactin beads (IBA Life Sciences) and allowed to bind for 2 hours.
203 Following purification, complexes bound to beads were washed and then eluted with desthiobiotin (IBA Life
204 Sciences). Proteins from cell lysates and AP eluates were evaluated by MS as below or separated by SDS-
205 PAGE and either directly stained using the Pierce Silver Stain Kit (Thermo Fisher Scientific) or transferred to a
206 PVDF membrane for immunoblotting.
207
208 AP eluates analyzed by MS underwent tryptic digest, desalting, and concentration and were then analyzed by
209 LC/MS-MS on a Thermo Scientific Velos Pro Linear Ion Trap MS system or a Thermo Scientific Q Exactive
210 Hybrid Quadrupole Orbitrap MS system equipped with a Proxeon EASY nLC II high-pressure liquid
211 chromatography and autosampler system. Raw data were searched against SwissProt human protein
212 sequences and the individual viral bait sequences using the Protein Prospector algorithm. PPIs were then scored
213 with MiST algorithm using previously defined conditions (0.309 for reproducibility, 0.75 for specificity, and 0.006
214 for abundance). Cytoscape was used for visualization of the PPI network (21).
215
216 We also performed AP-MS on human bait proteins in the presence or absence of HBx. For these experiments,
217 the bait proteins were cloned into the pcDNA4 vector with an N-terminal 3xFlag tag. These were transfected into
218 HUH7 with pcDNA4-eGFP or pcDNA-ST-HBx, and then AP performed as above, but with anti-Flag-M2 magnetic
219 beads (Sigma Aldrich, St. Louis MO). After washing, enriched proteins were eluted with Flag peptide and then
220 subjected to MS as above. After acquisition, data were again searched against SwissProt human protein

Downloaded from http://aacrjournals.org/cancerres/article-pdf/doi/10.1158/0008-5472.CAN-24-0456/3524752/can-24-0456.pdf by CDL - University of California - San Diego user on 10 January 2025

221 sequences. PPIs were scored with the MiST algorithm, as well as Saint (22) and Compass (23). A MiST score
222 of 0.7, Saint BFDR <0.05 and Compass p value < 0.05 were used in combination to define a rigorous set of high-
223 confidence PPIs; these were then overlaid onto the CORUM PPI map to define a strict PPI set. Label free protein
224 quantities were determined for each prey using MaxQuant (24), and statistical inference performed with Ms Stats
225 (25).
226

227 ## Network propagation

228 We first separately propagated the HBV deviances -- $D_{g_{hepB}}$, through the reference network. We retained the
229 propagated deviance scores in S_{d_g}. Conceptually, S_{d_g} indicates how likely it is that gene g is affected by proteins
230 with differential viral-associated mutations. Thus, we estimated the viral effect on human proteins within the
231 reference network by scoring the proximity of protein in the reference network to the HBV-interacting proteins at
232 genomic level.
233

234 Next, we separately propagated the HBV MiST scores through the reference network. The propagated MiST
235 scores were denoted by S_{p_g}. S_{p_g} represented the likelihood of gene g being affected by proteins that were
236 physically interacting with viral proteins. Thus, we estimated the viral effect on proteins within the reference
237 network, by scoring their proximity to the HBV-interacting proteins at physical level.
238

239 For network propagation, we used all human protein coding genes present in the reference network that were
240 also expressed in LIHC (p = 9,803 proteins). Given the topology of the reference network, there are certain nodes
241 (e.g. hubs) which will be 'hot' regardless of the initial scores represented by either deviances or MiST scores. To
242 estimate the expected background of the propagated scores given the network topology, we performed 10,000
243 permutations in which we randomly reassigned the deviances $D_{g_{hepB}}$, and the HBV MiST scores. To calculate
244 the significance of the propagation score of a specific gene, we ran the network propagation algorithm separately
245 with the permuted deviances and MiST scores as input scores and we calculated empirical *p* values. The *p*
246 values indicated how many times the propagated scores after permutation are greater than the real scores.
247

248 We used the gene-wise propagated MiST and deviances scores to calculate a combined measure of significance
249 for each protein coding gene. We defined the combined significance score as:
250 $$S_{c_g} = S_{d_g} * S_{p_g}.$$
251

252 To obtain the null hypothesis distribution of the combined score given the network topology, we performed 10,000
253 permutations through which we randomly reassigned MiST scores and deviances. We applied the network
254 propagation algorithm and calculated the product of the two propagated scores. We then calculated empirical *p*
255 values corresponding to the combined score. The *p* values indicated which genes had network neighborhoods
256 significantly enriched for both viral interactors and genes with differential mutation rates. We calculated the false
257 discovery rate using the Benjamini–Hochberg procedure (48). The values represented the probabilities of
258 erroneously finding genes with neighborhoods significantly enriched for both viral interactors and genes with
259 differential mutation rates. Next, we used the interactions in the reference network between the proteins that
260 showed combined significance and the viral-host interactions to build integrated interactomes of HBV in HCC
261 (Figure 3C). Our code is available on Github (https://github.com/adspit/HBV_HCC_interaction_inference).
262

263 ## Global phosphoproteomics

264 Huh7 cells with doxycycline-controlled 3xFLAG-HBx were treated with vehicle or doxycycline for 48 hours. Cells
265 were then harvested in PBS, lysed in lysis buffer (8uM urea, 50mM Tris pH 8, 75mM NaCl, 1X protease and
266 phosphatase inhibitors) and sonicated at 20% for 15 sec. Bicinchoninic acid (BCA) protein assay was performed
267 to quantify protein lysates. Samples were reduced, alkylated and subjected to trypsin digestion at 37C overnight.
268 Phosphopeptide enrichment was performed with immobilized metal affinity chromatography following

Downloaded from http://aacrjournals.org/cancerres/article-pdf/doi/10.1158/0008-5472.CAN-24-0456/3524752/can-24-0456.pdf by CDL - University of California - San Diego user on 10 January 2025

269 established protocols (26). Enriched samples were analyzed on a Q Exactive Orbitrap Plus mass spectrometry
270 system (Thermo Fisher Scientific). All mass spectrometry was performed at the Thermo Fisher Scientific
271 Proteomics Facility for Disease Target Discovery at UCSF and the J. David Gladstone Institutes. Mass
272 spectrometry data was assigned to human sequences and peptide identification and label-free quantification
273 were performed with MaxQuant (version 1.5.5.1)(27). Data were searched against the UniProt human protein
274 database (downloaded 2017). Statistical analysis was performed using the MSstats Bioconductor package (25).
275 Phosphoproteomic data was uploaded to the PhosFate profiler tool (28) (Phosfate.com) to infer kinase activity.
276

277 ### Multiplex inhibitor beads

278 Kinase chromatography, mass spectrometry and analytical processing were performed as described previously
279 (29). Bait compounds were purchased or synthesized and coupled to sepharose. Cell lysates were diluted in
280 binding buffer with 1 mol/L NaCl, and affinity purification was performed with gravity chromatography after pre-
281 clearing. The bound kinases were stringently washed and then eluted with SDS followed by
282 extraction/precipitation, tryptic digest and desalting. Liquid chromatography-tandem mass spectrometry (LC/MS-
283 MS) was performed on a Velos Orbitrap (Thermo Scientific) with in-line high-performance liquid chromatography
284 (HPLC) using an EASY-spray column (Thermo Scientific). Label-free quantification was performed with Skyline
285 (30), and statistical analysis with Ms Stats (25).
286

287 ### Western blots and antibodies

288 Cells were lysed with RIPA and Complete protease inhibitors and PhosStop phosphatase inhibitors following
289 standard techniques. Blots were cut to allow analysis of multiple proteins at different molecular weights, and
290 stripping was performed with Restore Western Blot stripping buffer (Thermo Fisher), to allow analysis of
291 phosphorylation and total expression. The majority of primary and secondary antibodies were obtained from Cell
292 Signaling (Danvers, MA) as follows: AKT (Cell Signaling Technology Cat# 9272, RRID:AB_329827), Phospho-
293 AKT S473 (Cell Signaling Technology Cat# 4060, RRID:AB_2315049), GAPDH (Cell Signaling Technology Cat#
294 2118, RRID:AB_561053), ILK (Cell Signaling Technology Cat# 3856, RRID:AB_2233861), MOB (Cell Signaling
295 Technology Cat# 13730, RRID:AB_2783010). Phospho-MOB T35 (Cell Signaling Technology Cat# 8699,
296 RRID:AB_11139998), PP2Ac (Cell Signaling Technology Cat# 2038, RRID:AB_2169495), Ribosomal protein S6
297 (Cell Signaling Technology Cat# 2217, RRID:AB_331355), Phospho-Ribosomal protein S6 S240/244 (Cell
298 Signaling Technology Cat# 2215, RRID:AB_331682), RICTOR (Cell Signaling Technology Cat# 2140,
299 RRID:AB_2179961), Phospho-RICTOR T1135 (Cell Signaling Technology Cat# 3806, RRID:AB_10557237),
300 Yap (Cell Signaling Technology Cat# 12395, RRID:AB_2797897), Phospho-YAP S127 (Cell Signaling
301 Technology Cat# 13008, RRID:AB_2650553). Actin (Sigma-Aldrich Cat# A2228, RRID:AB_476697), Flag
302 (Sigma-Aldrich Cat# F3165, RRID:AB_259529) and Flag-HRP (Sigma-Aldrich Cat# A8592, RRID:AB_439702)
303 were obtained from Sigma (St. Louis, MO), HBx (Abcam Cat# ab2741, RRID:AB_303266) and SMC5 (Abcam
304 Cat# ab18038, RRID:AB_2192782) were obtained from Abcam (Cambridge, MA). Strep (Thermo Fisher
305 Scientific Cat# MA5-17282, RRID:AB_2538748) was obtained from Thermo Fisher.
306

307 ### Quantitative Real Time PCR

308 RNA was extracted from cell lines with Trizol (Invitrogen). Reverse transcription was performed using the
309 Superscript II RT kit (Invitrogen) with random hexamer primers (Roche). 18S and beta-actin were used as
310 endogenous controls. All primers were generated with the Primer3 online tool (http://bioinfo.ut.ee/primer3);
311 sequences available on request. Quantification was performed using SYBR green labeling.
312

313 ### Immunohistochemistry

314 Analysis of mouse samples was performed on formalin fixed/paraffin embedded material with standard
315 techniques and staining performed with anti-Ki67 (Thermo Fisher Scientific Cat# MA5-14520,
316 RRID:AB_10979488; 1:150), followed by DAB development with Vectastain Elite ABC.
317

Downloaded from http://aacrjournals.org/cancerres/article-pdf/doi/10.1158/0008-5472.CAN-24-0456/3524752/can-24-0456.pdf by CDL - University of California - San Diego user on 10 January 2025

318 BrDU Incorporation
319 HUH7 or Hep3B cells were plated 1000 cells/well in black opaque bottom 96-well plates and BrdU cell
320 proliferation kit protocol (Exalpha, Shirley MA) was followed. Briefly, cells were allowed to attach for 48 hours
321 then BrdU at a final concentration of 10 μM was added for 2 hours. Cells were then fixed, washed and stained
322 according to manufacturer's protocol. Final absorbance at 450 nm was read.
323
324
325 Vectors and cloning
326 We used the following vectors to engineer cell models: pHR-SFFV-dCAS9-BFP-KRAB (RRID:Addgene_46911)
327 and pCRISPRia-v2 (RRID:Addgene_84832) was kindly provided by Luke Gilbert (UCSF). Gateway compatible
328 pLVX-TetOne-Puro (RRID:Addgene_171123) was described previously (31), and adapted to hygromycin
329 selection. HBV genes were PCR subcloned from the 1.3wt HBV construct (32), obtained from Addgene
330 (RRID:Addgene_65462), and all human proteins used in AP-MS were obtained from the Orfeome v8.1 (33).
331
332 CRISPRi
333 Targeted CRISPRi analysis was performed following established protocols. Briefly, cells expressing dCas9-
334 KRAB were sorted for BFP. dCas9-KRAB cells were then individually lentivirally infected with 3-5 sgRNAs
335 against the gene target and selected with puromycin. Gene knockdown was confirmed by quantitative real time
336 (QRT)-PCR, with sgRNA that failed to knockdown their target excluded from analysis. Proliferation of CRISPRi
337 cells was performed on a ZOOM Incucyte over 120 hours. Area under the curve (AUC) analysis of cell count or
338 confluence at each time point was developed and compared to cells transduced with a non-targeting control
339 (NTC) sgRNA.
340
341 expression correlation between proteins.
342
343 Data Availability Statement
344 The proteomics data have been deposited to the ProteomeXchange Consortium via the PRIDE partner
345 repository with the dataset identifier PXD055366. The Reverse Phase Protein Array (RPPA) expression data
346 from the TCGA Liver Cancer study analyzed in this study were obtained from the University of California, Santa
347 Cruz Xena Genome browser at https://xenabrowser.net.
348 Code is on Github: https://github.com/adspit/HBV_HCC_interaction_inference.
349
350
351 **Results**
352 HBV-HCC interactome
353 We first performed affinity purification - mass spectrometry (AP-MS) to identify HBV PPIs (6) in the HUH7
354 HCC line. While this line is derived from a patient without co-morbid HBV infection, it can generate intact HBV
355 virions from exogenous DNA (34,35), suggesting that it expresses all essential HBV-binding host proteins.
356 Further, given that these cells were not exposed to HBV during tumor initiation, any HBV PPIs that exert anti-
357 proliferative effects on HCC will not have been selected against. We used a 2X Strep epitope to tag and pull
358 down each HBV protein, including Pol, HBc and HBx. In addition, we separately examined the secreted HBc
359 variant e antigen (HBe) and short (SHB), medium (MHB) and long (LHB) isoforms of HBs (Fig. 1A). These were
360 overexpressed individually in HUH7 HCC cells, with AP performed using streptavidin beads. Co-purifying human
361 proteins were identified by MS and scored with MS interaction Statistics (MiST) software (20). Based on prior
362 publications with subsequently validated viral interactomes, we defined a MiST score threshold of 0.75, which
363 identified 145 total high-confidence PPIs (Fig. 1B; Table S1).
364 Functional analysis of the identified proteins with the Reactome database (36) revealed enrichment of
365 proteins involved in pre-mRNA processing (HBc), nucleotide excision repair and mTOR signaling (HBx) and the
366 unfolded protein response (HBe and LHB; Fig. 1C). The full map (Fig. 1D) included novel PPIs of HBV subunits
367 with biologically significant host proteins including eIF4H and DDX3X (HBc) as well as Prohibitin 1 and 2 (LHB,
368 SHB). It also included many known and suspected HBx interactions such as PRKAA1, PPP2CA, HDAC1, and
369 the CRL4 E3 ubiquitin ligase complex. Selected PPIs were confirmed by AP-western (Fig. S1), chosen based
370 on the results of the network propagation analysis below as well as their potential clinical actionability based

Downloaded from http://aacrjournals.org/cancerres/article-pdf/doi/10.1158/0008-5472.CAN-24-0456/3524752/can-24-0456.pdf by CDL - University of California - San Diego user on 10 January 2025

371 presence of small molecule inhibitors. This interaction network provides an expanded view of the potential effects
372 of HBV in HCC cells.
373

374 HBV significantly impacts gene mutation status in HCC

375 We next identified genes with differential mutational status relative to viral infection. We used Bayesian logistic
376 regression to identify protein-coding genes with recurrent genetic alterations in The Cancer Genome Atlas
377 (TCGA) HCC cohort (2) for which the alteration rate was significantly dependent on the presence of HBV or HCV
378 infection (Fig. 2A). This strategy allowed us to evaluate the impact of the two hepatitis viruses on a broad
379 spectrum of commonly and rarely mutated genes in HCC. We identified 70 genes with differential mutation based
380 on viral status (*p* value <0.05, FDR < 20%; Table S2). The majority of differentially mutated genes had increased
381 mutation frequency upon HBV viral infection (Fig. 2B). No statistically significant differences were observed in
382 HCV-associated HCC compared to the remaining subsets. Notably, the tumor suppressors *TP53* and *MAP2K4*
383 and the oncogene *GNAQ* were preferentially mutated in HBV+HCC, while the tumor suppressor *BAP1* was
384 preferentially mutated in non-HBV-associated HCC. These data expand on our prior work (10) and confirm an
385 impact of HBV on HCC genomes, but only provide partial insight into the ongoing role of HBV in HCC. Thus, we
386 next pursued further investigation into direct effects of HBV.
387

388 Network model integrates oncogenic HBV protein and genetic interactions

389 To stratify PPIs based on the likelihood that they exert oncogenic effects, we used a network-based strategy to
390 integrate HBV/host PPIs with differential HCC mutations, following the method established earlier for HPV (6).
391 Point mutations and copy number aberrations that were less frequent in HBV-associated HCC (in comparison to
392 HCV-associated and non-viral HCC) were used to identify mutations that might phenocopy HBV PPIs. This
393 analysis followed the rationale that increased incidence of a mutation in the absence of HBV could indicate an
394 important pathway in HCC that is directly modified by a PPI in HBV-associated tumors.
395 We applied statistical confidence measurements for our PPI and genomic data sets to the ReactomeFI
396 network, a public catalog of >200,000 pathway relationships among human proteins, including PPIs,
397 transcriptional regulatory interactions, and metabolic reactions. We used the framework of network propagation
398 (36). Deviances reflecting significance of differential mutation and MiST scores reflecting PPI confidence were
399 propagated separately across the network to generate a *p* value for each protein. Propagated *p* values were
400 combined, resulting in a set of 61 network nodes with FDR < 0.1, indicating Proximity in ReactomeFI to HCC
401 differential mutations and to HBV/host PPIs (Fig. 2C, Table S3). This set includes genes that did not meet our
402 confidence threshold to be considered HBV PPIs but through network proximity and/or differential mutation meet
403 the threshold of inclusion (Fig. S2A, shown in dark grey). This analysis allowed prioritization of a subset of the
404 HBV/host PPIs and added related genes to their local networks. For HBc, interactions with SRPK1 and FUS
405 were expanded to include KHSRP, ELAVL1 and PTBP1, giving a larger group of host factors with potential roles
406 in HBV's known effects on splicing (37). Conversely, network propagation did not expand the set of PPIs for
407 HBx. Instead, it allowed PPI prioritization based on cancer relevance, nominating COPS4, CUL4B, GART (a
408 purine synthesis enzyme), PPP2CA and PRKAA1 key HBx effectors.
409 A key objective of this study is to identify HBV PPIs that may result in targetable vulnerabilities in HBV
410 associated HCC. Given HBx's putative oncogenic role with anticipated effects on cell proliferation, we focused
411 on the HBV PPIs that were also significant by network propagation and assessed their impact on cell proliferation
412 with CRISPR interference with 5 independent sgRNA, using the essential gene Polo-like kinase 1 (PLK1) as a
413 positive control. Knockdown of *CUL4B*, *PPP2CA* and *PRKAA1* increased HUH7 proliferation, while knockdown
414 of *GART* and *COPS4* did not, showing a good concordance between our systems analysis and a relevant cancer
415 readout (Fig. 2D). The Hep3B cell line is derived from a patient with HBV and can also support HBV replication
416 (34), and was used for additional testing of the impact of HBx PPIs on cellular proliferation. In Hep3B, only
417 PPP2CA sgRNA increased cell proliferation, with a lower relative change than observed for HUH7 as confluence
418 rather than cell number was measured by real time microscopy (Fig. 2E). Thus, PP2A restrains proliferation in
419 both HUH7 and Hep3B. We further found that increased cell numbers correlated with increased BrDU
420 incorporation in HUH7 cells with *PPP2CA* knockdown (Fig. 2F). Knockdown was confirmed by QRT-PCR (Fig.
421 S2B).
422

423 HBx physically remodels host PP2A complexes

424 With these HBx/host PPIs prioritized based on their impact on cell proliferation, we next assessed the mechanism
425 by which HBx can act on these targets. While HBx interacts with components of the CRL4 E3 ubiquitin ligase
426 (e.g. CUL4B) and its regulator the COP9 signalosome (COPS4), the impact of HBx to redirect CRL4 degrading

Downloaded from http://aacrjournals.org/cancerres/article-pdf/doi/10.1158/0008-5472.CAN-24-0456/3524752/can-24-0456.pdf by CDL - University of California - San Diego user on 10 January 2025

427 activity towards the SMC5/6 complex is well described (12,13). Thus, we analyzed PP2A given its impact on
428 proliferation in both HUH7 and Hep3B. The HBx/PP2A interaction has been previously demonstrated, but
429 subsequent reports have shown different effects of HBx on distinct PP2A complexes (38-40). The PP2A
430 holoenzyme consists of PP2Ac, the scaffolding subunit PP2AA (gene *PPP2R1A*), and one of >15 regulatory
431 subunits. These subunits direct PP2Ac's substrate selection; several are tumor suppressors, including PPP2R4
432 and the PPP2R5 families (41). Thus, we hypothesized that HBx might alter PP2A's signaling effects via a
433 mechanism that is sensitive to PP2A's interactions with its regulatory subunits.
434 Accordingly, we performed quantitative AP-MS with the PP2A catalytic subunit (PP2Ac, gene *PPP2CA*)
435 in the presence or absence of HBx. The PP2A interactome showed significant changes in its interaction with
436 regulatory subunits in the presence of HBx (Fig. 3A; Table S4). HBx expression resulted in reduced interaction
437 between PP2Ac and PP2A regulatory subunits B alpha and delta (*PPP2R2A, PPP2R2D*), PP2A regulatory
438 subunit B' delta (*PPP2R5D*), STRN3 and STRN4. STRN3 and STRN4 are components of the Hippo pathway
439 regulating STRIPAK complex (42). HBx expression also resulted in reduced PP2Ac interaction with STRIPAK
440 components STRIP1 and MOB4, as well as the DDR proteins RAD23A/B (Fig. 3B).
441 First, to understand the mechanism of these differential effects we used truncations to define the
442 HBx/PP2Ac interaction surface and determined that HBx interacts with the first 108 amino acids of PP2Ac (Fig.
443 3C). This was modeled on the STRIPAK cryo-EM structure (43), showing that HBx binds to PP2Ac in a region
444 that positions it to block binding of STRN3 and displace its associated complex components (Fig. 3D).
445 The PP2A holoenzyme is made up of PP2Ac, a scaffolding subunit and PP2A regulatory subunits, which
446 direct PP2Ac's activity towards specific substrates. Thus, we used CRISPRi to prioritize the impact of different
447 PP2A complexes on HUH7 and Hep3B proliferation. Strikingly, we find that while *PPP2R2D*, *PPP2R5D* and
448 *STRN3* knockdown all increase HUH7 confluence, *STRN3* and *STRN4* knockdown increase Hep3B confluence
449 (Fig. 3E-F). These data support our prior results that HBV/host PPIs tend to inactivate growth inhibitory
450 mechanisms and nominate displacement of STRN3 from PP2A complexes as a key result of HBx/PP2Ac
451 interaction.
452
453 ## HBx modulates HCC signaling by disrupting PP2A effects
454 The interaction between HBx and PP2A suggests a mechanism by which HBV can regulate HCC
455 signaling. To understand HCC signaling in the context of basal HBx expression levels, we assessed a panel of
456 liver cancer cell lines from HBV positive (n=11) and negative (n=5) patients. HBx gene expression was assessed
457 by qPCR, with which we found that 8 of 11 HBV-associated HCC lines had detectable HBx levels (Table S5, Fig.
458 S3A). As a verification, we used PathSeq (10) to identify HBV sequences in RNA-Seq data available for 11 of
459 these lines and found perfect concordance with our qPCR results. We used QRT-PCR to determine expression
460 level of each PP2A regulatory subunit found to be displaced by HBx, and did not find a significant difference in
461 expression level across the panel (Fig. S3A), nor did cells cluster by HBV RNA expression (Fig. S3B).
462 We then performed kinome profiling using Multiplex Inhibitor Beads coupled with mass spectrometry
463 (MIB/MS) (29) to compare kinase expression and activity in HCC cells (Table S6). As MS detection is influenced
464 by kinase expression levels, MIBs have somewhat reduced detection of kinases with low abundance but favor
465 the measurement of kinases with poorly annotated targets. This dataset allowed us to assess whether
466 endogenous HBx expression might alter PP2A activity. We studied this relationship by correlating expression
467 levels of PP2A regulatory subunits whose presence in the holoenzyme is blocked by HBx (Fig. 3B) with signaling
468 of their known targets. As expected, we observed consistent negative correlation between regulatory subunit
469 expression and MIBs-determined kinase activity in non-HBx expressing cells, including PPP2R2D with CDK2,
470 PPP2R5D with FAK, and AMPKA2 with STRN3 (Fig. 4A). STRIP1 is a STRN3 interacting protein that is present
471 in MST1/2 regulating PP2A complexes (44). Expression of STRIP1 was significantly correlated with MST1/2
472 activity in non-HBx expressing cells (Fig. 4A), consistent with previous results (42). However, there was no
473 correlation between PP2A subunit expression and activity of these kinases in HBx-expressing lines. These data
474 suggested that HBx broadly disrupts signaling control by PP2A.
475
476 ## HBx effects on PP2A result in increased AKT and mTORC2 activation
477 We hypothesized that there may also be recurrently activated signals as a result of HBx effects on PP2A. Thus,
478 we used global phosphoproteomics to assess changes in cellular signaling pathways in HUH7 cells upon HBx
479 expression. Secondary analysis was performed with the Phosfate kinase attribution tool (28), which uses
480 annotated phosphopeptides to identify kinases with altered activity in the presence of HBx. These data showed
481 HBx-induced changes in motility, cell cycle/DNA damage, and stress and MAPK/PI3K pathways (Fig. 4B; Table
482 S7,8), including a significant increase in AKT activity (7). We note that the AKT3 paralog is specifically identified

Downloaded from http://aacrjournals.org/cancerres/article-pdf/doi/10.1158/0008-5472.CAN-24-0456/3524752/can-24-0456.pdf by CDL - University of California - San Diego user on 10 January 2025

483 as upregulated, although given the lack of clear differences in substrate selectivity between AKT1, 2 and 3 (45)
484 it is possible that this is an analytical artifact. Pro-motility signaling such as Myosin light-chain kinase (MYLK)
485 and p21-activated kinase 1 (PAK1) were also regulated. Notably, AKT exists in a feed-forward signaling loop
486 with one of its key regulators, mTOR complex 2 (mTORC2), the rapamycin-insensitive complex that contributes
487 to mTOR signaling, with known effects on metabolism and cell migration. As signaling from AKT and mTORC2
488 might be difficult to decouple using a signaling attribution tool, we also assessed our primary phosphoproteomics
489 results for a recently annotated set mTORC2 targets from glioblastoma (46). Despite being from a distinct tissue
490 type, we found this target set was significantly enriched in the phosphopeptides upregulated by HBx expression
491 (Fig. S3C, $p<0.001$ by Chi-square test).
492 We tested these observations by western blot in HUH7. Strikingly, HBx overexpression increased
493 activating phosphorylation of the essential mTORC2 scaffold RICTOR at T1135. Importantly, the same effect
494 was seen with the direct PP2Ac inhibitors LB-100 and okadaic acid (OA), with little additive impact of PP2A
495 inhibition and HBx overexpression. While total RICTOR levels also change, this is consistent with a known
496 stabilizing effect of this phosphorylation event (47). AKT phosphorylation was sufficiently low in HUH7 to be
497 inconsistently detected by western blot, so is not shown. STRN3-associated PP2A can inhibit the Hippo tumor
498 suppressor pathway via effects on the Hippo kinases MST1 and MST2 (42). Consistent with a loss of
499 PP2A/STRIPAK activity, we found that HBx overexpression results in increased phosphorylation but reduced
500 expression of the terminal Hippo target YAP, suggesting its downregulation by Hippo (Fig. 4C). We also note
501 that OA treated cells express higher levels of HBx, although it is unclear if this is a direct effect of OA on HBx
502 stability or on its expression from a plasmid.
503 Similar results were seen in HUH7 following *PPP2CA* knockdown, although we note that the sgRNA with
504 more significant PP2Ac reduction was also associated with reduced RICTOR phosphorylation, potentially due to
505 feedback effects due to chronic, rather than acute, PP2A downregulation (Fig. S3D). These findings were also
506 tested in SNU-475, an HBx-expressing HCC line which expresses similarly high levels of STRIPAK subunits to
507 HUH7 (Fig. S3B). Here, HBx overexpression did not dramatically impact Hippo signaling, as measured by MOB
508 expression and phosphorylation. However, it dramatically increased RICTOR phosphorylation as seen above
509 (Fig. 4C), with a more minimal effect on AKT phosphorylation (Fig. S3E). Suggesting that HBx effects on YAP
510 are at least partially post-translational, we observed that MG-132 rescued the effects of HBx expression on YAP
511 in HUH7 and Hep3B (Fig. S3F), and that HBx overexpression did not significantly alter YAP mRNA levels (Fig.
512 S3G).
513 We also looked for recurrent signaling alterations across our MIBs data set, where PP2A regulatory
514 subunit expression was more variable. As anticipated, the heterogeneity between cells in this larger collection
515 resulted in relatively few consistently altered kinases based on HBx expression. These included the
516 pseudokinase ILK, which is anticipated to still be detectable by MIBs via allosteric regulation of an ATP binding
517 site (48), as well as the pro-inflammatory kinase RIPK2 and the pro-motility kinase TNK2 (Fig. 4D). Notably, AKT
518 is relatively difficult to detect with MIBs (29) and was not identified in this analysis. ILK (49), RIOK2 (50), and
519 TNK2 (51) have all been shown to activate mTORC2 output. Thus, even in cell models which lack high levels of
520 STRN3, and thus are less likely to have significant activation of Hippo signaling, mTORC2 activation appears to
521 be a recurrent event in the presence of HBx (see schematic, Fig. 4E).
522
523 ## mTOR Complex 2 regulates of YAP in HCC
524 Although signaling can be visualized as a series of linear kinase relays, many pathways exist in complex
525 interconnected networks. Thus, the upregulation of the Hippo tumor suppressive kinase pathway raised the
526 possibility that another aspect of HBx-induced signaling remodeling may exert an opposing effect to maintain
527 YAP expression. Thus, we hypothesized that AKT and/or mTORC2 might influence YAP stability in HBx-
528 expressing cell models. To address this possibility in a line without significant STRN3 upregulation, we shifted
529 our experiments to the HBx+ Hep3B cells.
530 Consistent with results in HUH7, HBx overexpression and LB-100 treatment both reduced baseline YAP
531 levels in Hep3B, although mTORC2 upregulation was limited. Cells were also treated with the allosteric AKT
532 inhibitor MK2206 and the ATP-competitive mTORC1/mTORC2 mTOR inhibitor TAK-228 (sapanisertib). These
533 data showed reduced YAP protein levels with each compound, with TAK-228 having the greatest effect. All
534 effects were more pronounced in the presence of HBx (Fig. 5A), as seen above (Fig. 4C). As a parallel
535 confirmation, we used CRISPRi to reduce expression of the PSK ILK, finding that it decreased YAP levels
536 independent of HBx levels (Fig. S4).
537 We hypothesize that HBx accesses important cellular pathways rather than inducing them *de novo*, and
538 thus that mTORC2 effects on YAP can be potentiated by either HBx or other factors signaling to these pathways.

Downloaded from http://aacrjournals.org/cancerres/article-pdf/doi/10.1158/0008-5472.CAN-24-0456/3524752/can-24-0456.pdf by CDL - University of California - San Diego user on 10 January 2025

539 Thus, we next confirmed that TAK-228 treatment reduces YAP protein levels in the HBx-expressing cells SNU-
540 182 and SNU-449 as well as the non-HBx expressing line SNU 423 (Fig. 5B), which has high levels of ILK activity
541 based on the MIBs assay (Table S8). We confirmed that TAK-228's effect on YAP expression was due to
542 mTORC2 inhibition by comparing the effects of the allosteric mTORC1 inhibitor everolimus, the Rapalink
543 mTORC1 inhibitor (16) E-1035 and TAK-228 in SNU-182, observing that YAP levels are only reduced when
544 mTORC2 is inhibited. Furthermore, this effect was sensitive to the proteasomal inhibitor MG-132, suggesting
545 that mTORC2 acts on YAP degradation (Fig. 5C). Notably, MG-132 did slightly decrease pAKT and AKT levels,
546 as has been previously described (52). Consistent with post-transcriptional YAP regulation, reduced mRNA
547 expression of canonical YAP targets was also observed following TAK-228 treatment in cell lines, while YAP
548 mRNA was not significantly changed (Fig. 5D).
549 To confirm this observation *in vivo* and validate the role of mTORC2 as a regulator of YAP in HCC, we
550 tested the impact of *Rictor* deletion in an Akt/Ras-driven murine HCC model. Here, we found that Cre-mediated
551 *Rictor* deletion resulted in longer survival compared to pT3 empty vector, with robust induction of aggressive
552 tumors when Rictor was intact and improved survival in the absence of Rictor (Fig. 6A). When confirming *Rictor*
553 deletion, we saw near elimination of YAP expression, as well as reduced but persistent Akt pS473 (Fig. 6B).
554 Reduced YAP levels correlated with reduced proliferation by Ki-67 staining (Fig. 6C). These findings show that
555 mTORC2 contributes to YAP regulation *in vivo* and again support its effect in the absence of HBx. These data
556 suggest that the balance between Hippo and mTORC2 signaling control YAP expression in HCC. Consistent
557 with this idea, we noted close correlation between levels of mTORC2 activation based on RICTOR pT1135 and
558 YAP in HBV RNA+ and non-HBV RNA expressing specimens in TCGA. We also found that YAP and AKT pS473
559 were strongly inversely correlated in this data set (Fig. 6D), further supporting our finding that mTORC2 effects
560 on YAP, are independent of AKT. Thus, rather than creating *de novo* signaling effects, HBx remodels a kinase
561 network around the control of YAP levels, acting in parallel to augmenting an inhibitory signal (Hippo) that results
562 in YAP phosphorylation and degradation as well as an activating signal (AKT/mTORC2) which maintains YAP
563 expression even if it has been phosphorylated (Fig. 6E).
564
565 **Discussion**
566 This work describes the first complete HBV/HCC protein-protein and genomic interactome, and refinement of
567 our network propagation strategy to identify cancer-relevant PPIs in genetically heterogeneous context of HCC.
568 Our tiered analytical strategy allowed us to define remodeling of PP2A as an important HBV effector function,
569 which appears to at least partially overcome a proliferative block applied by STRN3 containing PP2A complexes.
570 Further, the increase in Hippo pathway activity resulting from HBx effects on STRN3/PP2A complexes may result
571 in a dependency on mTORC2 function to maintain YAP protein levels. The significant alterations of PP2A
572 function and the HCC kinome in the presence of HBx suggest that this may be one of several signaling
573 dependencies emerging in the context of HBV infection. Further, mTORC2's maintenance of YAP expression in
574 non-HBx-expressing specimens supports our model that HBV acts through cellular pathways that also support
575 non-HBV-associated HCC.
576
577 This work advances the use of network strategies and multi-modality integrative models to study viral effects on
578 cancer and reinforces the importance of protein interaction networks in defining disease-relevant genetic
579 relationships (31,53). The mutations in non-HBV HCC that identified oncogenic HBV PPIs are not focused on a
580 single oncogene or tumor suppressor, but rather occur across multiple members of a protein complex. By using
581 network propagation, we were able to decode these relationships in an unbiased fashion and identify biologically
582 meaningful relationships. This will likely broaden the utility of this strategy for the many other tumor associated
583 viruses with indirect effects (54). Similarly, the integration of gene expression with proteomic data sets to assess
584 the impact of HBx on PP2A interaction partners and downstream signaling allowed for the identification of a clear
585 pattern of effects in multiple cell models.
586
587 Given the paucity of targeted therapy options for HCC, we focus here on signaling alterations that are driven by
588 effects on PP2A. Viral disruption of PP2A function is common, with displacement of cancer-relevant regulatory
589 subunits also seen in the context of the SV40 small T antigen (55), although HBx effects on PP2A do not appear
590 to directly drive HCC proliferation. A broad array of viruses can influence PP2A activity in other ways to support
591 their replication, including HCV which has been shown to express a PP2A regulatory subunit that can direct
592 holoenzyme activity to inhibit inflammatory signaling (56). The remodeling of the PP2A complex by HBx
593 decoupled it from the regulation of multiple cellular signaling pathways, most notably disrupting its inhibition of
594 the Hippo tumor suppressor by STRN3/PP2A complexes and thus and decreasing YAP protein expression. This

Downloaded from http://aacrjournals.org/cancerres/article-pdf/doi/10.1158/0008-5472.CAN-24-0456/3524752/can-24-0456.pdf by CDL - University of California - San Diego user on 10 January 2025

apparently growth inhibitory effect of HBx can be countered by mTORC2, which can maintain YAP protein levels by blocking its degradation. While prior studies have also shown that HBx can increase YAP mRNA expression (57,58), this effect of mTORC2 occurs even in the absence of HBx and is confirmed in mouse models and RPPA data from human HCC, suggesting it is a robust mechanism that may interact with the other mechanisms by which HBx augments YAP activity in HCC. We also note that mTORC2 has been shown to directly phosphorylate YAP at Serine 436. This may be the mechanism by which it stabilizes YAP (59), but we were unable to detect this phosphorylation by phosphoproteomics and there is no antibody publicly available to test it.

Limitations: This study provides proof of concept for applying systems strategies to HBV and other viruses with indirect cancer promoting effects. One key potential limitation is the development of our AP-MS data in the HUH7 cell line, derived from a patient lacking HBV infection and previously used to develop the HCV PPI map (15). This line is one of three capable lines derived from patients without HBV that are nevertheless capable of supporting HBV replication, even though only a subset of lines derived from patients with HBV maintain HBV gene expression (Fig. S4) and replication (34). The loss of HBV gene expression in these latter lines suggests that in vitro culture adaptation may select against HBV replication potentially by downregulating interacting proteins.

HBx effects on PP2A and its impact on HCC signaling are just one of many potential HBV-induced effects on HCC biology, and we have focused on tumor cell intrinsic effects of HBV proteins, rather than those that may impact the HCC/microenvironment interaction. Similarly, while we provide valuable systems level data about HBV effects, some details are uncertain and may need to be validated as part of future studies (e.g., the identification of AKT3 as opposed to other AKT family members in phosphoproteomics, Fig 4B). Further, while our study highlights a relationship between HBx effects on PP2A and sensitivity to mTORC1/2 inhibitors, it does not provide evidence of preferential activity of mTORC1/2 inhibitors in HBV-associated HCC models. That analysis will require larger scale studies, such as the Phase 2 study of the mTORC1/mTORC2 inhibitor ATG-008 in HBV-associated HCC (NCT03591965) and may depend on co-occurrence of HBV infection and high level expression of STRN3. Similarly, additional study would be required to understand if HBx exerts oncogenic effects in *Rictor*$^{-/-}$ mice, and how YAP is regulated in that context.

In summary, our analysis provides comprehensive maps of the physical and genetic interactions between HBV and HCC, using computational methods to integrate these maps and nominate mechanisms by which HBV alters the behavior of HCC. Our validation of PP2A as one such mechanism supports the overall strength of our strategy, and future investigation can be used to assess a number of other targets of interest. Further, as large scale genomic datasets are analyzed in more depth, our estimate of the rate of direct viral infection of tumors is increasing to well over 10% (60,61). Our finding that HBV exerts ongoing effects on fundamental HCC processes encourages the application of this refined analytical strategy to the many other cancer-associated viruses.

References

1. Sung H, Ferlay J, Siegel RL, Laversanne M, Soerjomataram I, Jemal A*, et al.* Global Cancer Statistics 2020: GLOBOCAN Estimates of Incidence and Mortality Worldwide for 36 Cancers in 185 Countries. CA Cancer J Clin **2021**;71:209-49
2. Cancer Genome Atlas Research Network. Electronic address wbe, Cancer Genome Atlas Research N. Comprehensive and Integrative Genomic Characterization of Hepatocellular Carcinoma. Cell **2017**;169:1327-41 e23
3. Totoki Y, Tatsuno K, Covington KR, Ueda H, Creighton CJ, Kato M*, et al.* Trans-ancestry mutational landscape of hepatocellular carcinoma genomes. Nat Genet **2014**;46:1267-73
4. Gordan JD, Kennedy EB, Abou-Alfa GK, Beal E, Finn RS, Gade TP*, et al.* Systemic Therapy for Advanced Hepatocellular Carcinoma: ASCO Guideline Update. J Clin Oncol **2024**;42:1830-50
5. Kim RD, Sarker D, Meyer T, Yau T, Macarulla T, Park JW*, et al.* First-in-Human Phase I Study of Fisogatinib (BLU-554) Validates Aberrant FGF19 Signaling as a Driver Event in Hepatocellular Carcinoma. Cancer Discov **2019**;9:1696-707
6. Eckhardt M, Zhang W, Gross AM, Von Dollen J, Johnson JR, Franks-Skiba KE*, et al.* Multiple Routes to Oncogenesis Are Promoted by the Human Papillomavirus-Host Protein Network. Cancer Discov **2018**;8:1474-89
7. Levrero M, Zucman-Rossi J. Mechanisms of HBV-induced hepatocellular carcinoma. J Hepatol **2016**;64:S84-S101

Downloaded from http://aacrjournals.org/cancerres/article-pdf/doi/10.1158/0008-5472.CAN-24-0456/3524752/can-24-0456.pdf by CDL - University of California - San Diego user on 10 January 2025

651 8. Li Y, Tang ZY, Hou JX. Hepatocellular carcinoma: insight from animal models. Nat Rev Gastroenterol
652 Hepatol **2011**;9:32-43
653 9. Arbeit JM, Munger K, Howley PM, Hanahan D. Progressive squamous epithelial neoplasia in K14-human
654 papillomavirus type 16 transgenic mice. J Virol **1994**;68:4358-68
655 10. Lim HC, Gordan JD. Tumor hepatitis B virus RNA identifies a clinically and molecularly distinct subset of
656 hepatocellular carcinoma. PLoS Comput Biol **2021**;17:e1008699
657 11. Nassal M. HBV cccDNA: viral persistence reservoir and key obstacle for a cure of chronic hepatitis B.
658 Gut **2015**;64:1972-84
659 12. Decorsiere A, Mueller H, van Breugel PC, Abdul F, Gerossier L, Beran RK*, et al.* Hepatitis B virus X
660 protein identifies the Smc5/6 complex as a host restriction factor. Nature **2016**;531:386-9
661 13. Murphy Christopher M, Xu Y, Li F, Nio K, Reszka-Blanco N, Li X*, et al.* Hepatitis B Virus X Protein
662 Promotes Degradation of SMC5/6 to Enhance HBV Replication. Cell Reports **2016**;16:2846-54
663 14. Sekiba K, Otsuka M, Funato K, Miyakawa Y, Tanaka E, Seimiya T*, et al.* HBx-induced degradation of
664 Smc5/6 complex impairs homologous recombination-mediated repair of damaged DNA. J Hepatol
665 **2022**;76:53-62
666 15. Ramage HR, Kumar GR, Verschueren E, Johnson JR, Von Dollen J, Johnson T*, et al.* A combined
667 proteomics/genomics approach links hepatitis C virus infection with nonsense-mediated mRNA decay.
668 Mol Cell **2015**;57:329-40
669 16. Rodrik-Outmezguine VS, Okaniwa M, Yao Z, Novotny CJ, McWhirter C, Banaji A*, et al.* Overcoming
670 mTOR resistance mutations with a new-generation mTOR inhibitor. Nature **2016**;534:272-6
671 17. Chen X, Calvisi DF. Hydrodynamic transfection for generation of novel mouse models for liver cancer
672 research. Am J Pathol **2014**;184:912-23
673 18. Reva B, Antipin Y, Sander C. Predicting the functional impact of protein mutations: application to cancer
674 genomics. Nucleic Acids Res **2011**;39:e118
675 19. Gelman A, Jakulin A, Pittau MG, Su YS. A Weakly Informative Default Prior Distribution for Logistic and
676 Other Regression Models. Ann Appl Stat **2008**;2:1360-83
677 20. Jager S, Gulbahce N, Cimermancic P, Kane J, He N, Chou S*, et al.* Purification and characterization of
678 HIV-human protein complexes. Methods **2011**;53:13-9
679 21. Shannon P, Markiel A, Ozier O, Baliga NS, Wang JT, Ramage D*, et al.* Cytoscape: a software
680 environment for integrated models of biomolecular interaction networks. Genome Res **2003**;13:2498-504
681 22. Choi H, Larsen B, Lin ZY, Breitkreutz A, Mellacheruvu D, Fermin D*, et al.* SAINT: probabilistic scoring of
682 affinity purification-mass spectrometry data. Nat Methods **2011**;8:70-3
683 23. Sowa ME, Bennett EJ, Gygi SP, Harper JW. Defining the human deubiquitinating enzyme interaction
684 landscape. Cell **2009**;138:389-403
685 24. Cox J, Mann M. MaxQuant enables high peptide identification rates, individualized p.p.b.-range mass
686 accuracies and proteome-wide protein quantification. Nat Biotechnol **2008**;26:1367-72
687 25. Choi M, Chang CY, Clough T, Broudy D, Killeen T, MacLean B*, et al.* MSstats: an R package for statistical
688 analysis of quantitative mass spectrometry-based proteomic experiments. Bioinformatics **2014**;30:2524-
689 6
690 26. Budzik JM, Swaney DL, Jimenez-Morales D, Johnson JR, Garelis NE, Repasy T*, et al.* Dynamic post-
691 translational modification profiling of Mycobacterium tuberculosis-infected primary macrophages. Elife
692 **2020**;9
693 27. Tyanova S, Temu T, Cox J. The MaxQuant computational platform for mass spectrometry-based shotgun
694 proteomics. Nat Protoc **2016**;11:2301-19
695 28. Ochoa D, Jonikas M, Lawrence RT, El Debs B, Selkrig J, Typas A*, et al.* An atlas of human kinase
696 regulation. Mol Syst Biol **2016**;12:888
697 29. Donnella HJ, Webber JT, Levin RS, Camarda R, Momcilovic O, Bayani N*, et al.* Kinome rewiring reveals
698 AURKA limits PI3K-pathway inhibitor efficacy in breast cancer. Nat Chem Biol **2018**;14:768-77
699 30. Schilling B, Rardin MJ, MacLean BX, Zawadzka AM, Frewen BE, Cusack MP*, et al.* Platform-independent
700 and label-free quantitation of proteomic data using MS1 extracted ion chromatograms in skyline:
701 application to protein acetylation and phosphorylation. Mol Cell Proteomics **2012**;11:202-14
702 31. Kim M, Park J, Bouhaddou M, Kim K, Rojc A, Modak M*, et al.* A protein interaction landscape of breast
703 cancer. Science **2021**;374:eabf3066
704 32. Wang H, Kim S, Ryu WS. DDX3 DEAD-Box RNA helicase inhibits hepatitis B virus reverse transcription
705 by incorporation into nucleocapsids. J Virol **2009**;83:5815-24

Downloaded from http://aacrjournals.org/cancerres/article-pdf/doi/10.1158/0008-5472.CAN-24-0456/3524752/can-24-0456.pdf by CDL - University of California - San Diego user on 10 January 2025

706 33. Rual JF, Venkatesan K, Hao T, Hirozane-Kishikawa T, Dricot A, Li N, *et al.* Towards a proteome-scale
707 map of the human protein-protein interaction network. Nature **2005**;437:1173-8
708 34. Bhat SA, Ahanger IA, Kazim SN. Forthcoming Developments in Models to Study the Hepatitis B Virus
709 Replication Cycle, Pathogenesis, and Pharmacological Advancements. ACS Omega **2023**;8:14273-89
710 35. Ren S, Nassal M. Hepatitis B virus (HBV) virion and covalently closed circular DNA formation in primary
711 tupaia hepatocytes and human hepatoma cell lines upon HBV genome transduction with replication-
712 defective adenovirus vectors. J Virol **2001**;75:1104-16
713 36. Fabregat A, Jupe S, Matthews L, Sidiropoulos K, Gillespie M, Garapati P, *et al.* The Reactome Pathway
714 Knowledgebase. Nucleic Acids Res **2018**;46:D649-D55
715 37. Duriez M, Mandouri Y, Lekbaby B, Wang H, Schnuriger A, Redelsperger F, *et al.* Alternative splicing of
716 hepatitis B virus: A novel virus/host interaction altering liver immunity. J Hepatol **2017**;67:687-99
717 38. He C, Qiu Y, Han P, Chen Y, Zhang L, Yuan Q, *et al.* ER stress regulating protein phosphatase 2A-
718 B56gamma, targeted by hepatitis B virus X protein, induces cell cycle arrest and apoptosis of
719 hepatocytes. Cell Death Dis **2018**;9:762
720 39. Tsunematsu S, Suda G, Yamasaki K, Kimura M, Izumi T, Umemura M, *et al.* Hepatitis B virus X protein
721 impairs alpha-interferon signaling via up-regulation of suppressor of cytokine signaling 3 and protein
722 phosphatase 2A. J Med Virol **2017**;89:267-75
723 40. Gong SJ, Feng XJ, Song WH, Chen JM, Wang SM, Xing DJ, *et al.* Upregulation of PP2Ac predicts poor
724 prognosis and contributes to aggressiveness in hepatocellular carcinoma. Cancer Biol Ther **2016**;17:151-
725 62
726 41. Perrotti D, Neviani P. Protein phosphatase 2A: a target for anticancer therapy. Lancet Oncol
727 **2013**;14:e229-38
728 42. Shi Z, Jiao S, Zhou Z. STRIPAK complexes in cell signaling and cancer. Oncogene **2016**;35:4549-57
729 43. Jeong BC, Bae SJ, Ni L, Zhang X, Bai XC, Luo X. Cryo-EM structure of the Hippo signaling integrator
730 human STRIPAK. Nat Struct Mol Biol **2021**;28:290-9
731 44. Tang Y, Chen M, Zhou L, Ma J, Li Y, Zhang H, *et al.* Architecture, substructures, and dynamic assembly
732 of STRIPAK complexes in Hippo signaling. Cell Discov **2019**;5:3
733 45. Johnson JL, Yaron TM, Huntsman EM, Kerelsky A, Song J, Regev A, *et al.* An atlas of substrate
734 specificities for the human serine/threonine kinome. Nature **2023**;613:759-66
735 46. Kalpongnukul N, Bootsri R, Wongkongkathep P, Kaewsapsak P, Ariyachet C, Pisitkun T, *et al.*
736 Phosphoproteomic Analysis Defines BABAM1 as mTORC2 Downstream Effector Promoting DNA
737 Damage Response in Glioblastoma Cells. J Proteome Res **2022**;21:2893-904
738 47. Gao D, Wan L, Inuzuka H, Berg AH, Tseng A, Zhai B, *et al.* Rictor forms a complex with Cullin-1 to
739 promote SGK1 ubiquitination and destruction. Mol Cell **2010**;39:797-808
740 48. Fukuda K, Gupta S, Chen K, Wu C, Qin J. The pseudoactive site of ILK is essential for its binding to
741 alpha-Parvin and localization to focal adhesions. Mol Cell **2009**;36:819-30
742 49. McDonald PC, Oloumi A, Mills J, Dobreva I, Maidan M, Gray V, *et al.* Rictor and integrin-linked kinase
743 interact and regulate Akt phosphorylation and cancer cell survival. Cancer Res **2008**;68:1618-24
744 50. Read RD, Fenton TR, Gomez GG, Wykosky J, Vandenberg SR, Babic I, *et al.* A kinome-wide RNAi
745 screen in Drosophila Glia reveals that the RIO kinases mediate cell proliferation and survival through
746 TORC2-Akt signaling in glioblastoma. PLoS Genet **2013**;9:e1003253
747 51. Mahajan K, Coppola D, Chen YA, Zhu W, Lawrence HR, Lawrence NJ, *et al.* Ack1 tyrosine kinase
748 activation correlates with pancreatic cancer progression. Am J Pathol **2012**;180:1386-93
749 52. Zanotto-Filho A, Braganhol E, Battastini AM, Moreira JC. Proteasome inhibitor MG132 induces selective
750 apoptosis in glioblastoma cells through inhibition of PI3K/Akt and NFkappaB pathways, mitochondrial
751 dysfunction, and activation of p38-JNK1/2 signaling. Invest New Drugs **2012**;30:2252-62
752 53. Zheng F, Kelly MR, Ramms DJ, Heintschel ML, Tao K, Tutuncuoglu B, *et al.* Interpretation of cancer
753 mutations using a multiscale map of protein systems. Science **2021**;374:eabf3067
754 54. Tang KW, Alaei-Mahabadi B, Samuelsson T, Lindh M, Larsson E. The landscape of viral expression and
755 host gene fusion and adaptation in human cancer. Nat Commun **2013**;4:2513
756 55. Guergnon J, Godet AN, Galioot A, Falanga PB, Colle JH, Cayla X, *et al.* PP2A targeting by viral proteins:
757 a widespread biological strategy from DNA/RNA tumor viruses to HIV-1. Biochim Biophys Acta
758 **2011**;1812:1498-507
759 56. Duong FH, Filipowicz M, Tripodi M, La Monica N, Heim MH. Hepatitis C virus inhibits interferon signaling
760 through up-regulation of protein phosphatase 2A. Gastroenterology **2004**;126:263-77

Downloaded from http://aacrjournals.org/cancerres/article-pdf/doi/10.1158/0008-5472.CAN-24-0456/3524752/can-24-0456.pdf by CDL - University of California - San Diego user on 10 January 2025

761 57. Zhang T, Zhang J, You X, Liu Q, Du Y, Gao Y, *et al.* Hepatitis B virus X protein modulates oncogene
762 Yes-associated protein by CREB to promote growth of hepatoma cells. Hepatology **2012**;56:2051-9
763 58. Wu Y, Zhang J, Zhang H, Zhai Y. Hepatitis B virus X protein mediates yes-associated protein 1
764 upregulation in hepatocellular carcinoma. Oncol Lett **2016**;12:1971-4
765 59. Holmes B, Benavides-Serrato A, Saunders JT, Kumar S, Nishimura RN, Gera J. mTORC2-mediated
766 direct phosphorylation regulates YAP activity promoting glioblastoma growth and invasive characteristics.
767 Neoplasia **2021**;23:951-65
768 60. Zapatka M, Borozan I, Brewer DS, Iskar M, Grundhoff A, Alawi M, *et al.* The landscape of viral
769 associations in human cancers. Nat Genet **2020**;52:320-30
770 61. Elbasir A, Ye Y, Schaffer DE, Hao X, Wickramasinghe J, Tsingas K, *et al.* A deep learning approach
771 reveals unexplored landscape of viral expression in cancer. Nat Commun **2023**;14:785
772

773 **Figure Legends:**

774 **Figure 1: HBV-HCC protein interactome. A)** Map of the HBV genome with the outline of individual genes;
775 genes are overlapping with distinct reading frames. Individual genes are shown below in linear format to indicate
776 the length of each gene tested. **B)** Number of high-confidence PPIs for each HBV protein. **C)** Selected results of
777 bioinformatic analysis of HBV PPIs using the Reactome pathway database. **D)** HBV interactome. Solid edges
778 connect host proteins to the interacting HBV bait, while dashed lines show known human:human PPIs.
779 Functional subsets and known protein complexes are investigator identified and designated with a grey
780 background; n=2 biological replicates with 2 technical replicates per sample.
781

782 **Figure 2: HBV-HCC genetic interactome. A)** Differential mutation analysis: Bayesian logistic regression was
783 applied to 8,765 individual non-synonymous somatic mutations identified in the TCGA LIHC project to determine
784 the predictive effect of HBV or HCV, or either infection, on the rate of each individual mutation. Viral status was
785 determined based on clinical annotation. **B)** Deviance in HBV and mutation rate increased in HBV (positive) or
786 increased in non-HBV vs. HBV (negative). All genes with a mutation rate above 5% in HBV-associated or non-
787 HBV-associated HCC, with rates between 5-10% in blue and greater than 10% shown in red. **C)** Scatter plot of
788 network propagation distributed by the propagated p value for relative mutation vs. propagated p value for
789 significance of HBV PPI. All nodes with FDR < 10% are labeled, and those that interact directly with an HBV
790 protein are color coded by the HBV protein they bind. **D)** Analysis of HBx PPIs that are also significant from
791 network propagation for effects on cellular proliferation measured by nuclear counting: HUH7 cells were
792 engineered to express dCAS9-KRAB and then stably transduced with 4-5 sgRNA against each HBV PPI that
793 reached significance in network analysis; PLK1 is included as an essential gene control. Effects on proliferation
794 with real time microscopy over 120 hours are shown (* $p < 0.05$); n=3 biological replicates per sgRNA with a
795 minimum of 3 technical replicates per sample. Area under the curve (AUC) analysis of cell count at each time
796 point was developed and compared to cells transduced with a non-targeting control (NTC) sgRNA. **E)**
797 Assessment of impact of HBx PPIs significant by network-propagation on proliferation in Hep3B. Analysis
798 performed as in (D) above, with cell confluence measured in place of cell count. * $p < 0.05$, $n \geq 2$ biological
799 replicates per sgRNA with a minimum of 3 technical replicates per sample. **F)** ELISA-based assessment of BrDU
800 incorporation in HUH7 cells following PPP2CA knockdown. Results are from 2 biological replicates and a
801 minimum of 3 technical replicates per sample normalized to NTC (*$p < 0.05$).
802

803 **Figure 3: HBx remodels the PP2A holoenzyme. A)** AP-MS of the PPP2CA complex in HUH7 cells with co-
804 transfection of Flag-PPP2CA and Strep-HBx vs. Flag-PPP2CA and empty vector (EV). High confidence PPIs
805 are shown, with statistically significant changes in abundance in color; proteins of interest directly labeled. **B)**
806 Cytoscape presentation of AP-MS results from (A). Proteins with significantly altered abundance are shown in
807 color. There were no PPIs with increased abundance. **C)** Deletion mapping of the HBx/PPP2CA interaction with
808 co-overexpression; for PPP2CA Δ1, aa1-108 are deleted: PPP2CA Δ2, aa109-189 are deleted; PPP2CA Δ3,
809 aa190-310 are deleted. Biotin IP was used for complex purification and compared to whole cell lysate (WCL).
810 HBx binding is lost by deletion of aa 1-108. **D)** Model of the HBx/PPP2CA interaction and its physical proximity
811 to the PPP2CA/STRN3 interface overlaid onto the 7K36 cryo-EM structure. **E)** Impact of HBx-displaced PP2A
812 subunits on HUH7 proliferation measured by confluence. HUH7 dCAS9-KRAB cells were stably transduced with
813 ≥2 sgRNA against each PP2A subunit displaced by HBx, with PPP2CA knockdown shown as a benchmark.
814 Effects on proliferation with real time microscopy over 120 hours are shown (* $p < 0.05$); n=2 biological replicates
815 per sgRNA with a minimum of 3 technical replicates per sample. Area under the curve (AUC) analysis at each
816 time point was developed and compared to cells transduced with a non-targeting control (NTC) sgRNA. QRT-

Downloaded from http://aacrjournals.org/cancerres/article-pdf/doi/10.1158/0008-5472.CAN-24-0456/3524752/can-24-0456.pdf by CDL - University of California - San Diego user on 10 January 2025

817 PCR confirmed knockdown. **F)** Impact of HBx-displaced PP2A subunits on Hep3B proliferation as shown in **(E).**
818
819 **Figure 4: HBx alters HCC signaling by disrupting PP2A effects. A)** Correlation between PP2A component
820 expression and individual kinase activity in a panel of 16 HCC lines, including 8 with detectable HBx mRNA
821 expression; kinase activity determined using multiplex inhibitor beads (MIBs)/mass spectrometry (MS). In these
822 cases, HBx expression decouples PP2A subunit expression from activation of it's PP2A complex's target kinase.
823 **B)** Volcano plot of significant alterations in imputed kinase activation based on Phosfate analysis of global
824 phosphoproteomics of HUH7 cells with doxycycline-induction of HBx for 48 hours. **C)** Effect of HBx expression
825 on PP2A/STRIPAK target phosphorylation: HUH7 parental cells were transfected with pCDNA4 (EV) or HBx-ST
826 overnight and then treated with 50 nM okadaic acid (OA), 10 μM LB-100 (LB) or vehicle for 4 hours, resulting in
827 altered phosphorylation and expression of RICTOR, MOB1 and YAP. **D)** Significantly altered kinase activity
828 across our 16 HCC lines panel comparing cells with vs. without detectable HBx mRNA expression; kinase activity
829 determined using MIBs/ MS; p values derived using t tests. **E)** Overall model for HBx effects on signaling: In the
830 absence of HBx expression, PP2A function is determined by its typical upstream regulation mechanisms as well
831 as the overall expression of its regulatory subunits (left). However, when HBx is present, its interaction with
832 PPP2CA selectively disrupts PP2A function towards many targets, but does augment Hippo, mTORC2 and
833 motility signaling (right).
834
835 **Figure 5: HBx stabilization of YAP via mTORC2. A)** Impact of HBx on regulation of YAP expression by AKT
836 and mTOR. Hep3B cells with tet-inducible FL-HBx were treated with dox for 48 hours and then 1 mM MK-2206
837 or 100 nM TAK-228 or 10 μM LB-100 for 4 hours. n=2 biological replicates with 1 technical replicate per condition.
838 **B)** Effect of DMSO or 20, 100 or 500 nM TAK-228 treatment for 24 hours on YAP expression in HBx+ SNU-182
839 and SNU-449 HCC lines or HBx- SNU-423 line assessed by immunoblot. n=3 biological replicates with 1
840 technical replicate per condition. **C)** Relative impact of mTORC1 and mTORC2 on YAP degradation: SNU-182
841 cells were treated for 4 hours with 100 nM everolimus, 100 nM of the Rapalink mTORC1 inhibitor E-1035, 100
842 nM TAK-228, 10 μM MG-132 or TAK-228+MG-132. n=3 biological replicates with 1 technical replicate per
843 condition **D)** qPCR expression analysis of SNU-182 and SNU-449 cells of canonical YAP targets following 100
844 nM TAK-228 treatment for 4 hours, normalized to DMSO treated cells; * $p<0.05$ as determined by t-test; n=3
845 biological replicates with 3 technical replicate per condition.
846
847 **Figure 6: mTORC2 controls YAP in HCC *in vivo*. A)** Kaplan-Meyer survival analysis of *Rictor*$^{fl/fl}$ mice following
848 hydrodynamic tail vein injection with Akt, Ras and empty vector or Akt/Ras/Cre. Akt/Ras/Vector mice were
849 sacrificed at 5 weeks because of evident morbidity, and Akt/Ras/Cre sacrificed over time up to 22 weeks.
850 Characteristic images of livers at necroscopy. **B)** Immunoblot analysis of Rictor, Yap, mTORC2 target Akt S473
851 phosphorylation in *Rictor*$^{fl/fl}$ livers transduced with empty vector or Cre, and then Akt/Ras or Akt/Ras/Cre tumors
852 macrodissected at necroscopy. n=2 biological replicates with 3 technical replicate per condition. **C)** Quantified
853 Ki-67 staining in Akt/Ras/Vector and Akt/Ras/Cre mice. **D)** Pearson correlation between RICTOR pT1135 or AKT
854 pS473 and total YAP protein levels in HBV-associated and non-HBV associated HCC by RPPA from the TCGA
855 LIHC project. **E)** Summary of model, showing parallel effects of HBx acting on PP2A-regulated cellular pathways
856 to activate Hippo and mTORC2 signaling, resulting in maintained YAP expression.

Downloaded from http://aacrjournals.org/cancerres/article-pdf/doi/10.1158/0008-5472.CAN-24-0456/3524752/can-24-0456.pdf by CDL - University of California - San Diego user on 10 January 2025

Figure 1

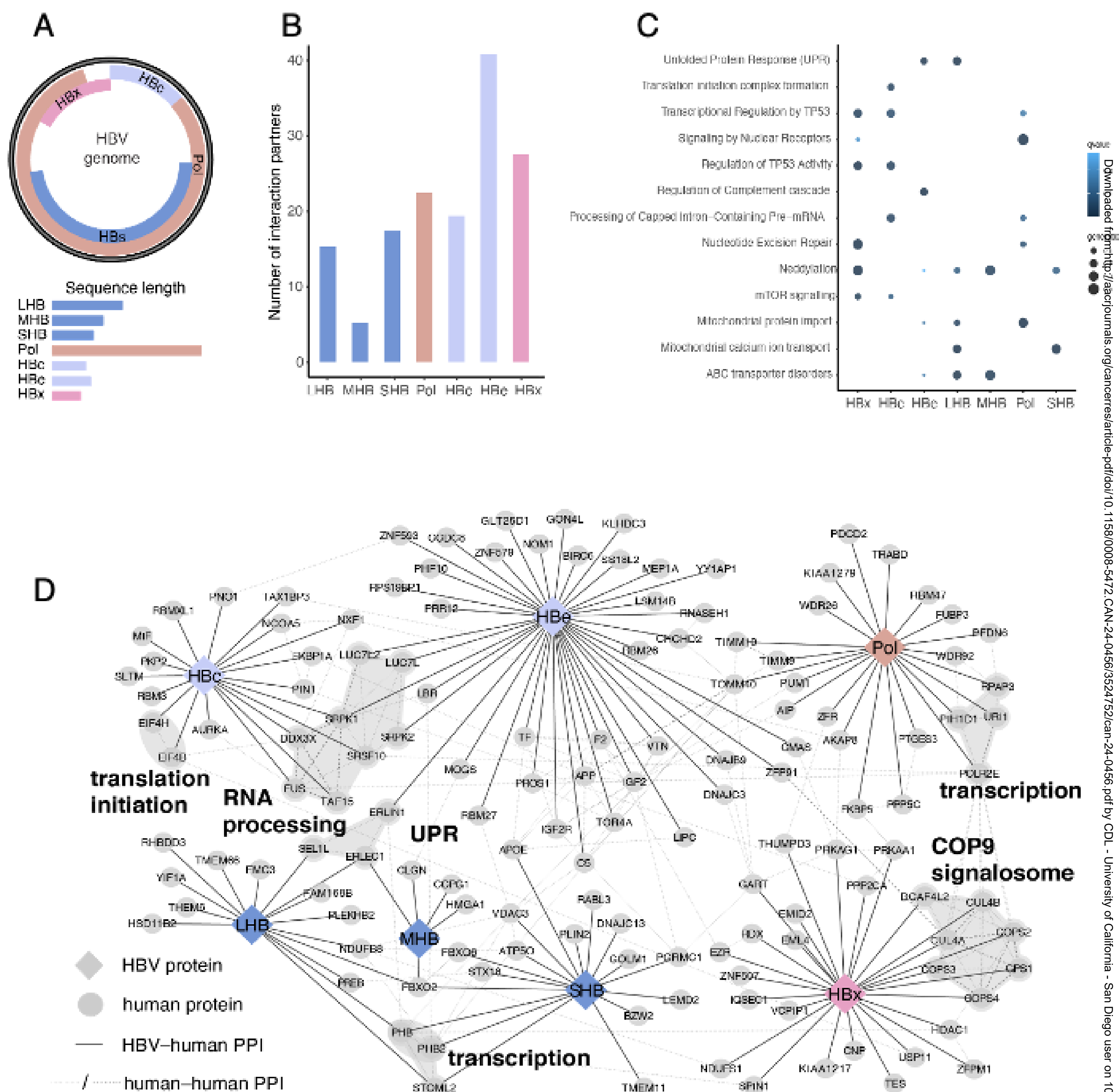

Downloaded from http://aacrjournals.org/cancerres/article-pdf/doi/10.1158/0008-5472.CAN-24-0456/3524752/can-24-0456.pdf by CDL - University of California - San Diego user on 10 January 2025

Figure 2

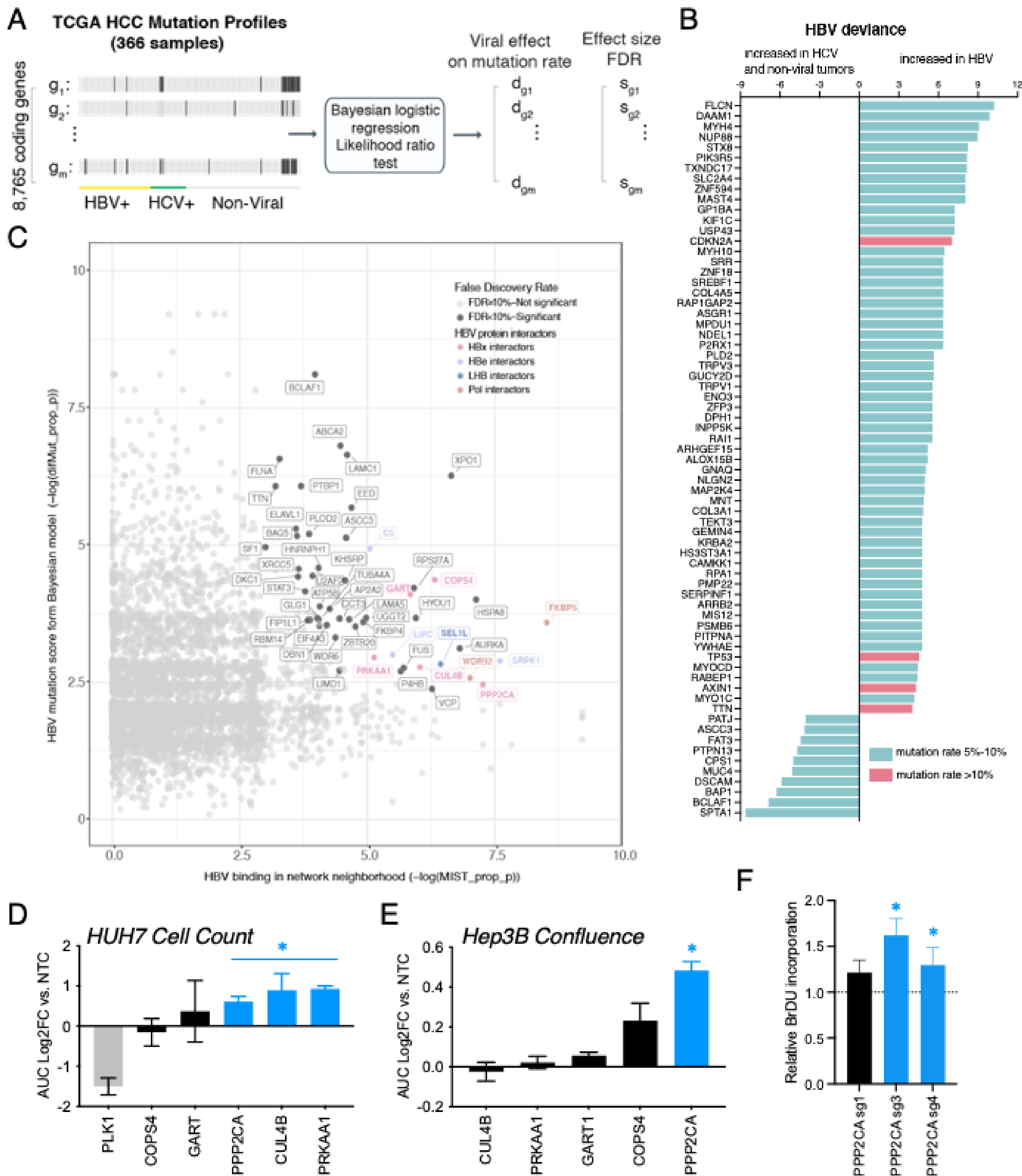

Downloaded from http://aacrjournals.org/cancerres/article-pdf/doi/10.1158/0008-5472.CAN-24-0456/3524752/can-24-0456.pdf by CDL - University of California - San Diego user on 10 January 2025

Figure 3

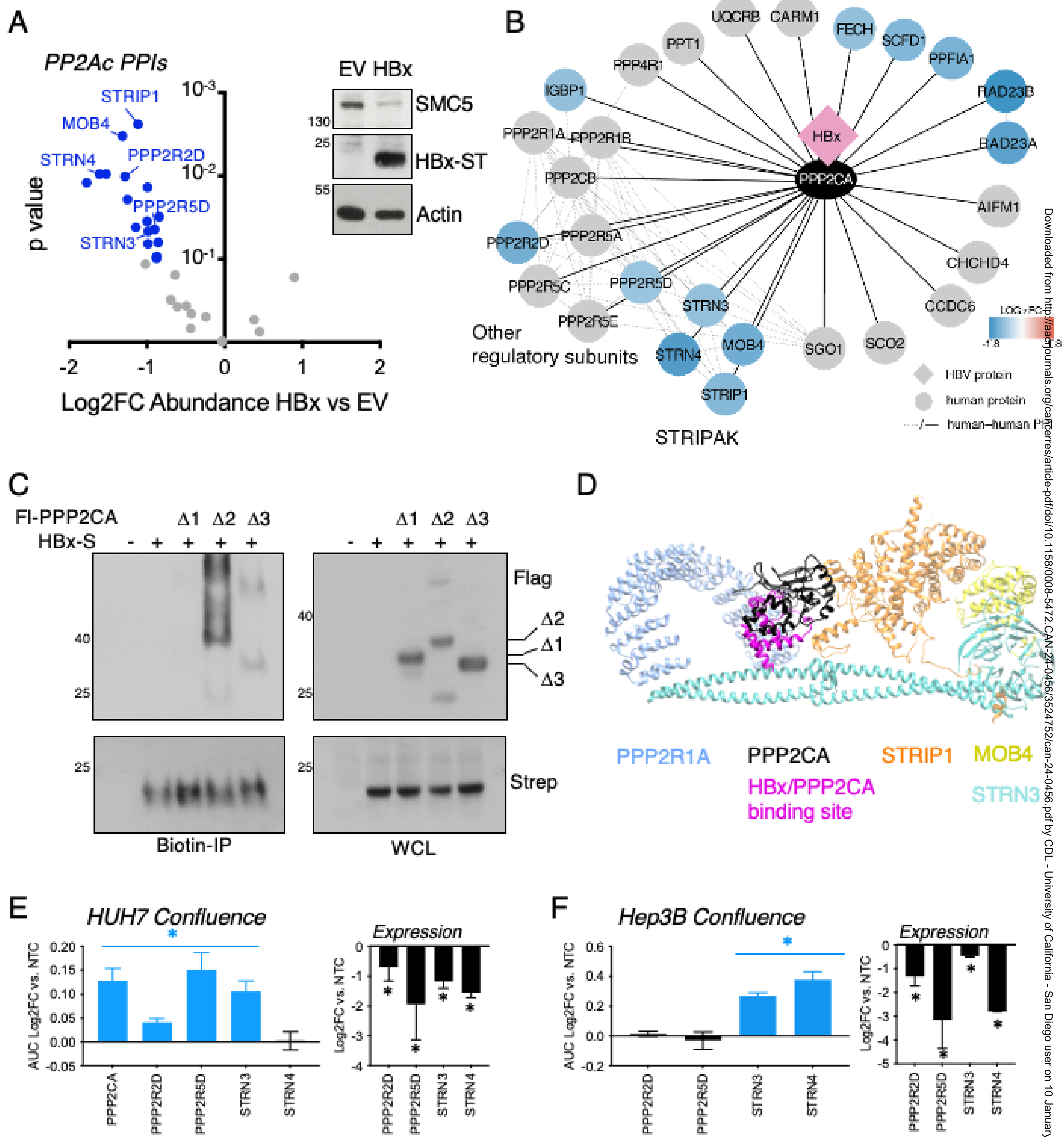

Downloaded from http://aacrjournals.org/cancerres/article-pdf/doi/10.1158/0008-5472.CAN-24-0456/3524752/can-24-0456.pdf by CDL - University of California - San Diego user on 10 January 2025

Figure 4

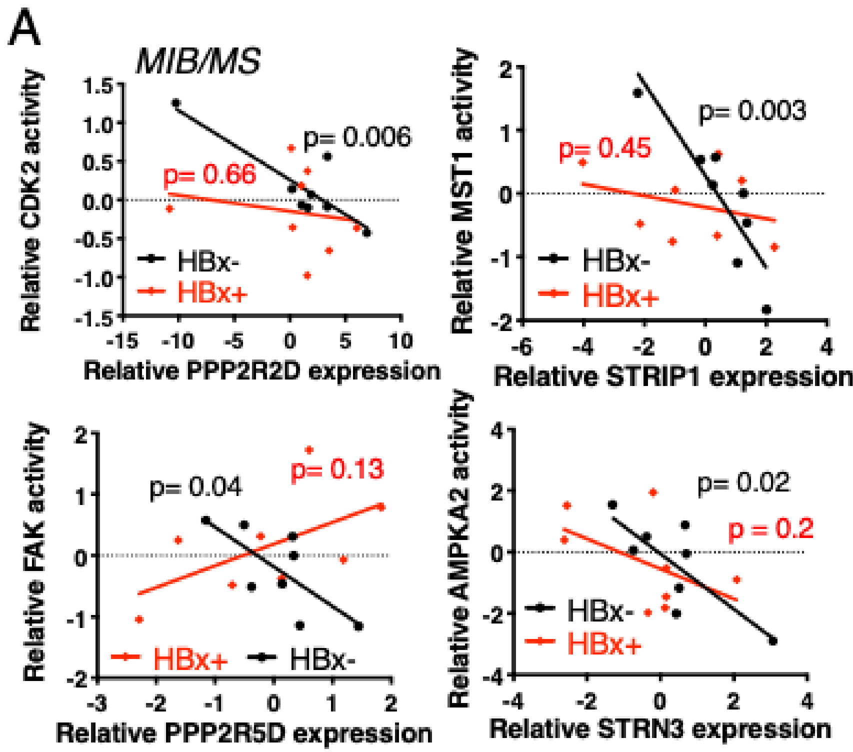

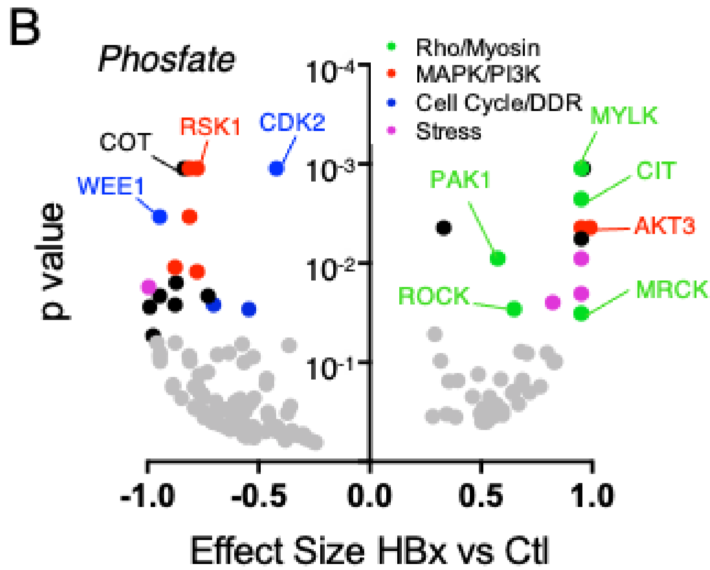

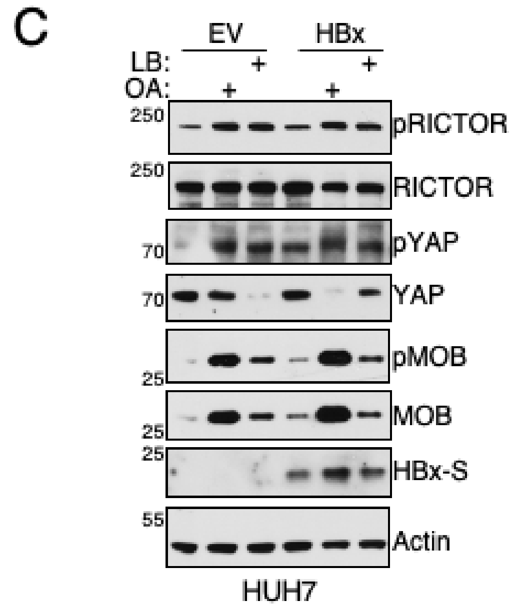

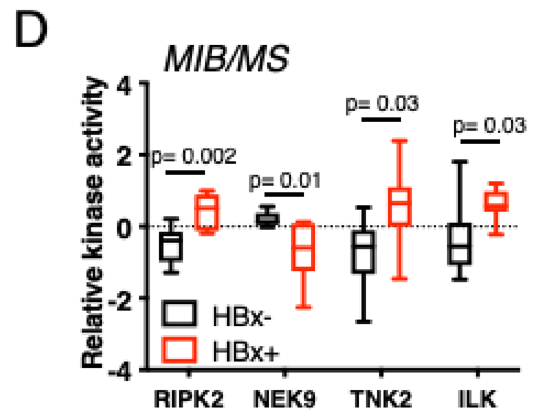

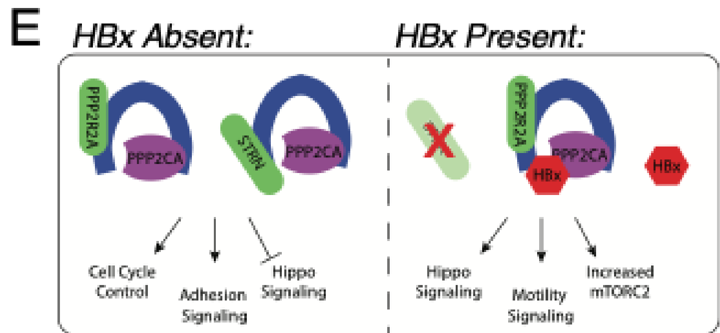

Downloaded from http://aacrjournals.org/cancerres/article-pdf/doi/10.1158/0008-5472.CAN-24-0456/3524752/can-24-0456.pdf by CDL - University of California - San Diego user on 10 January 2025

Figure 5

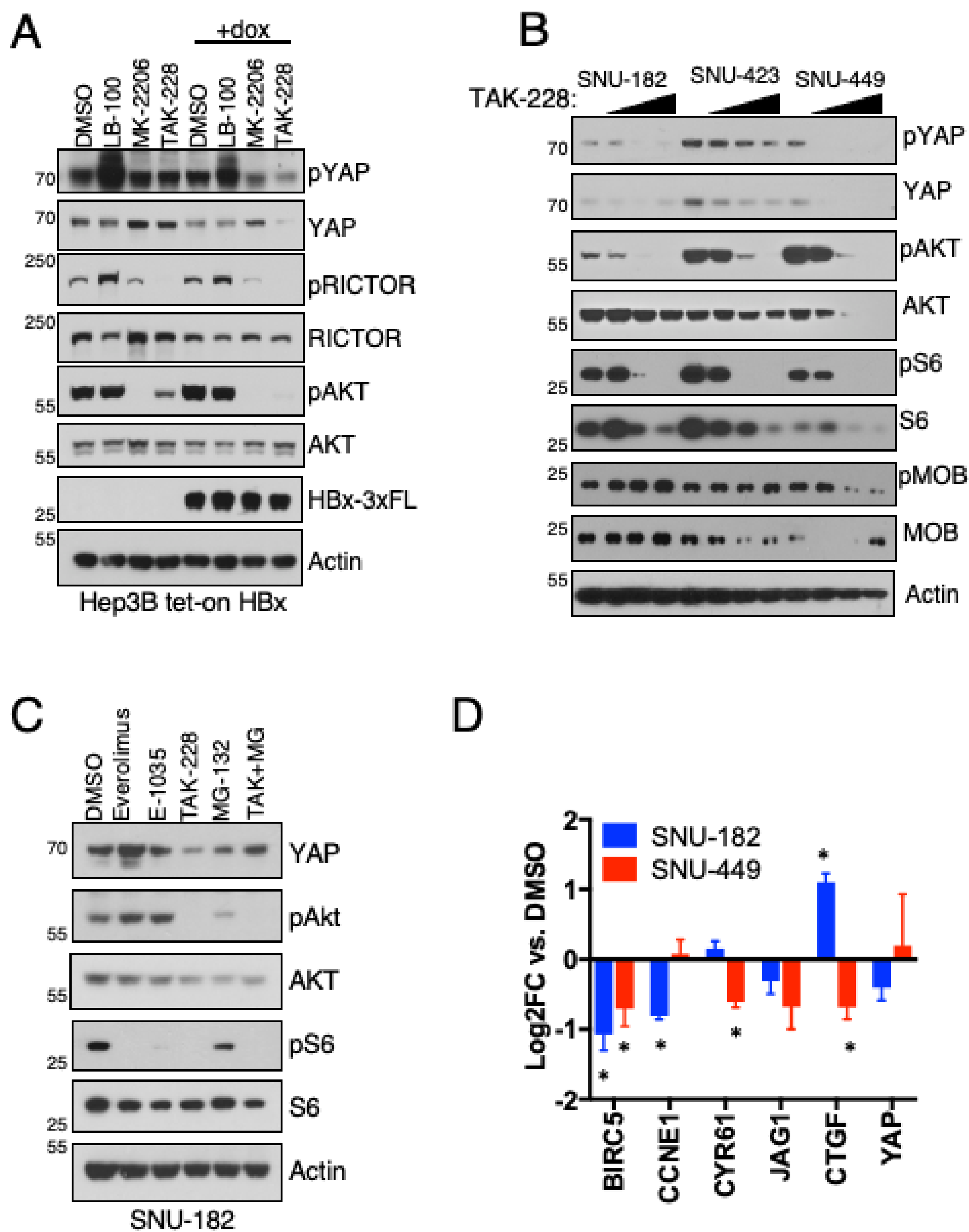

Downloaded from http://aacrjournals.org/cancerres/article-pdf/doi/10.1158/0008-5472.CAN-24-0456/3524752/can-24-0456.pdf by CDL - University of California - San Diego user on 10 January 2025

Figure 6

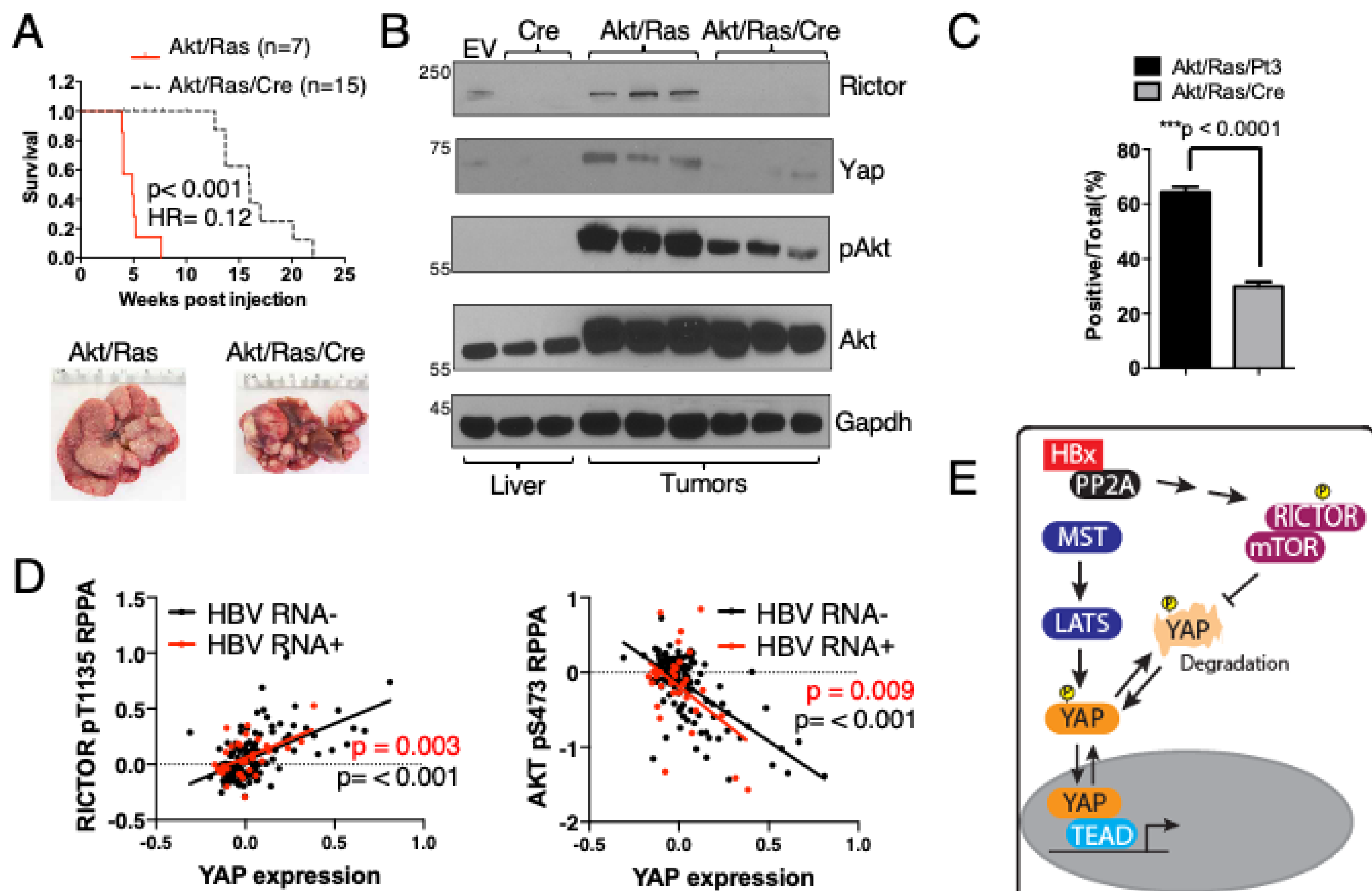

Downloaded from http://aacrjournals.org/cancerres/article-pdf/doi/10.1158/0008-5472.CAN-24-0456/3524752/can-24-0456.pdf by CDL - University of California - San Diego user on 10 January 2025